Article:
Maqbool, F, Abbas, SZ, Ramirez-Solis, S et al. (2 more authors) (2021) Modelling of one-dimensional heterogeneous catalytic steam methane reforming over various catalysts in an adiabatic packed bed reactor. International Journal of Hydrogen Energy, 46 (7). pp. 5112-5130. ISSN 0360-3199

https://doi.org/10.1016/j.ijhydene.2020.11.071

Modelling of one-dimensional heterogeneous catalytic steam methane reforming over various catalysts in an adiabatic packed bed reactor

Fahad Maqbool[a, b], Syed. Z. Abbas[a, c*], Sergio Ramirez-Solis[d], Valerie Dupont[d], Tariq Mahmud[d]

[a] Department of Chemical Engineering, University of Engineering and Technology, Lahore, Pakistan

[b] Department of Chemical Engineering, Sharif College of Engineering and Technology, Lahore, Pakistan

[c] Department of Chemical Engineering & Analytical Science, The University of Manchester, Manchester M13 9PL, United Kingdom

[d] School of Chemical and Process Engineering (SCAPE), University of Leeds, Leeds LS2 9JT, United Kingdom

Abstract

Kinetic data relevant to steam methane reforming (SMR) are often applied to catalysts and conditions from which they have not been derived. In this work, kinetic rates for the two SMR and water gas shift reactions were derived for 12 commonly used reforming catalysts based on conversion data obtained from the literature. Subsequently, these rates were tested in dynamic operation, steady-state, and equilibrium using a 1-D reactor model developed in-house with gPROMS model builder. Modelling outputs were further validated independently at equilibrium using the software chemical equilibrium with applications (CEA), and the literature. The effect of variables such as temperature, pressure, steam to carbon ratio (S/C), and gas mass flux (G_s) on the performance of the SMR process was then studied in terms of fuel and steam conversion (%), H_2 purity (%), H_2 yield (wt. % of CH_4) and selectivity of the carbon-based products. A comparative study was then performed for the 12 catalysts. Some catalysts showed better activity owing to their fast kinetics when they are tested in mild industrial conditions, while others performed better in more severe industrial conditions, substantiating that the choice of a catalyst ought to depend on the operating conditions.

Keywords: Steam methane reforming; Kinetics; Modelling; Chemical equilibrium; Catalyst

*Corresponding Author

Tel.: +447307858155

E-mail address: syedzaheer.abbas@manchester.ac.uk

1. Introduction

High energy consumption, finite fossil fuel reserves, and environmental concerns impel the research community to search for efficient and environment friendly alternatives to meet our increasing energy demands [1]. Because of their continuous depletion, limited nature, and non-homogeneous distribution, fossil fuels are getting scarce and their prices are gearing up [2]. Therefore, we are in dire need to shift away from carbon dioxide intensive processes and to switch to non-fossil fuel energy sources [3]. In this context, hydrogen (H_2) emerges as a clean energy vector and it has received great interest as a green fuel recently [4]. Without polluting the environment, H_2 can be used directly to drive the internal combustion (IC) engines or indirectly to generate electricity using fuel cells [1]. H_2 has a wide range of applications industrially, domestically, and in space technology [5]. At present, H_2 is predominantly employed in petroleum refining and petrochemicals, fertilizer industry, methanol production, and somewhat to a lesser extent in metal refining [6]. Primarily, H_2 is being consumed for ammonia and other nitrogenated fertilizers synthesis, hydrocracking and hydrotreating processes. It is also used for hydrogenation of food and hazardous wastes, synthesis of alcohols and ethers, gas to liquid synthesis technology (GTL), rocket fuel, and also as a potential fuel in IC engines and industrial furnaces [7]. The combustion of H_2 only engenders the emission of water vapors without the direct emission of any greenhouse gas [8].

The processes used for H_2 production are conventional thermochemical technologies (gasification, pyrolysis, reforming, thermochemical cycles), conventional electrochemical technologies (electrolysis, cold/hot plasma, photo-electrochemical), and biological/biochemical technologies (photosynthetic and fermentative) [9]. Approximately, 95 % of the worldwide produced H_2 comes from fossil fuel-based processes mainly employing natural gas (NG), coal, and crude oil [10]. NG, naphtha, petroleum coke, coal, and water are common feedstocks used for H_2 production, but currently, NG is the dominant H_2 source [11]. The various routes available for H_2 production using NG include steam methane reforming (SMR), partial oxidation (POx), and autothermal reforming (ATR). Despite their negative impact on the environment and contribution to global warming through the emission of greenhouse gases, SMR is at present leading in the production of H_2. SMR now contributes to almost 50% of the world's H_2 production [12-14].

The conventional SMR process comprises two main steps: the first step involves the conversion

of CH_4 to H_2 and CO in a reformer where the SMR reaction (R1) occurs at an elevated temperature (800 – 950 °C) and mild pressure (20 - 35 atm), followed by the second step at lower temperatures (200 - 400 °C) where conversion of carbon monoxide (CO) and steam to carbon dioxide (CO_2) and H_2 via the water-gas shift (WGS) reaction (R2) under medium pressure conditions takes place [15-17].

$$CH_{4(g)} + H_2O_{(g)} \rightleftharpoons CO_{(g)} + 3H_{2(g)} \qquad \Delta H_{rxn,298K} = 206.3 \text{ kJ mol}_{CH_4}^{-1} \qquad \text{(R1)}$$

$$CO_{(g)} + H_2O_{(g)} \rightleftharpoons CO_{2(g)} + H_{2(g)} \qquad \Delta H_{rxn,298K} = -41.1 \text{ kJ mol}_{CO}^{-1} \qquad \text{(R2)}$$

R1 is strongly endothermic in nature and as such is favored at high temperature, while the mildly exothermic R2 is thermodynamically favorable under lower temperature conditions, which explains their physical separation to obtain optimal conversions in the industrial process. The global reforming reaction (R3) is, as a result, still highly endothermic and thus the combined SMR process requires external heating. The R3 is given by [18];

$$CH_{4(g)} + 2H_2O_{(g)} \rightleftharpoons CO_{2(g)} + 4H_{2(g)} \qquad \Delta H_{rxn,298K} = 164.9 \text{ kJ mol}_{CH_4}^{-1} \qquad \text{(R3)}$$

Although, SMR is a well-established method for large scale hydrogen production but the main challenge is to reduce the overall environment and energy penalties associated with the CO_2 capturing and valorization technologies [19]. Reducing carbon emissions is of vital importance to tackle the climate changes and to decrease the carbon footprint of modern societies [20]. Both R1 and R2, are equilibrium limited, and it is impossible to achieve complete conversion of the CH_4 and CO in a single reactor. However, if the CO_2 can be removed from the gas phase as it is formed, the equilibrium can be shifted in forward direction and complete conversion can be closely approached [21]. In the sorption-enhanced steam reforming of methane (SER) hydrogen production process, hydrocarbon reforming, water gas shift, and CO_2 separation reactions occur simultaneously in a single reaction step over a reforming catalyst mixed with a CO_2 sorbent. Carbonation reaction (R4) with CaO as a sorbent is given by [22];

$$CO_{2(g)} + CaO_{(s)} \rightleftharpoons CaCO_{3(s)} + 4H_{2(g)} \qquad \Delta H_{rxn,298K} = -178.8 \text{ kJ mol}_{CaO}^{-1} \qquad \text{(R4)}$$

The overall SE-SMR reaction (R5) using CaO would become slightly exothermic in nature so that

no supplementary energy is required for the hydrogen production.

$$CH_{4(g)} + CaO_{(s)} + 2H_2O_{(g)} \rightleftharpoons CaCO_{3(s)} + 4H_{2(g)} \quad \Delta H_{rxn,298K} = -13.7\ kJ\ mol_{CaO}^{-1} \qquad (R5)$$

A number of studies have been carried by several authors in the literature to describe the benefits of SER by using various feedstocks and sorbents along with the different flow configurations and innovative processes combining sorption enhanced and chemical looping [23-36].

The SMR is a quite complex process, and thus, numerous efforts have been made in recent years aiming at the development of the most suitable catalyst to maximize the production of syngas [37]. In terms of catalytic activity, various authors have reported well-performing catalysts, thus, it has been very complicated to provide a specific order of performance. However, Jones et al. [38] proposed the following catalytic activity order: Ruthenium (Ru) > Rhodium (Rh) > Iridium (Ir) > Platinum (Pt), indicating Pt as the least active metal compared to the others. Although these noble metals are highly active and have a low presence of carbon deposition, the nickel-based (Ni) catalysts are so far the best and most used catalysts at the industrial scale for the SMR process [39]. Ni presents high activity, low attrition, and albeit it is expensive in comparison to other available choices among transition metals, the cost is minimized by using lower Ni content [40, 41].

The performance of the SMR process and product distribution is influenced by several factors including operating conditions (temperature, pressure, S/C), catalyst type, and reformer design features. Various studies have been carried out to investigate the kinetics of SMR reactions. The first extensive kinetic study was performed using Ni catalysts supported on kieselguhr at atmospheric pressure and in the temperature range of 335 – 635 °C. There was no kinetic mechanism suggested, but it was concluded that both CO and CO_2 were primary reaction products [42]. Numaguchi and Kikuchi [43] determined the intrinsic kinetics of SMR process over a nickel catalyst at temperatures varying from 674 K to 1160 K, pressure ranging from 1.2 to 25.5 bar, and feed molar steam to carbon ratio (S/C) between 1.44 and 4.50. They used an integral flow reactor, which was a fixed-bed model, found that surface reactions were the rate determining steps (RDS) with only CO as the primary reaction product. Xu and Froment [44] developed a kinetic model of SMR over a spinel Ni/$MgAl_2O_4$ catalyst for a temperature window of 500 – 670 °C, and surface reactions were considered to be the RDS in their proposed mechanism. Soliman et al. [45] studied

the intrinsic kinetics of SMR over a Ni/calcium aluminate catalyst. They proposed a mechanism comparable to Xu and Froment [44] but with CO_2 as the primary product that is then converted to CO through the reverse reaction R2. A kinetic model for the SMR in the temperature range of 500 – 600 °C, was proposed by Luna and Becerra [46] over a commercial Ni on alumina-titania catalyst with a Ni content of 22.9 wt. %. Hou and Hughes [47] also performed experiments to study the kinetics of SMR and the reverse WGS reaction by using commercial Ni/α-Al_2O catalyst with NiO content of 15-17 wt. % and in the temperature range of 475 – 550 °C under conditions of non-diffusion limitation. The results gave rise to a kinetic model with surface reactions being the RDS.

In the literature, there exist several models developed for SMR reactors ranging from pseudo-homogeneous to heterogeneous models, operated in a steady state and dynamic way. The SMR model development began in the 1960s. McGreavy and Newmann [48] proposed a steady-state SMR model of a top-fired reformer and compared the outputs of their model with real data (industrial plant). Later, they modified the model for dynamic simulation. Singh and Saraf [49] developed a 1-D steady-state homogeneous SMR model for a side-fired furnace and modified it for un-steady state simulation. Xu and Froment [50] used the kinetics that accounted for diffusional limitations in a 1-D heterogeneous model to simulate a commercial reformer. Soliman et al. [51], using the kinetic rate expressions obtained by Xu and Froment [44], developed a 1-D heterogeneous model and the model performance was tested against industrial reformers. Murty and Murthy [52] formulated a model of a top-fired reformer, this was validated with operating reformer data, and then, they performed a sensitivity analysis to identify the variables affecting the performance of SMR reformer. Plehiers and Froment [53] developed a 1-D heterogeneous model for side-fired SMR reformer, which was validated with industrial results and could predict the temperature distribution and effluent composition into the furnace. Recently, Yu et al. [54] performed 1-D pseudo-homogeneous modelling, compared the simulation outputs with the operating reformer data, and optimized the performance of the reformer. Shayegan et al. [55] developed a rigorous 2-D mathematical model, investigated the steady-state operation of an industrial Midrex™ reformer, and compared the outputs of 1-D and 2-D models. They also explained how the catalyst-loading profile affects the reformer performance. Ebrahimi et al. [56] validated the model of a top fired NG reformer against the industrial and literature data, and investigated the effect of important process variables on the performance of SMR reformer. Olivieri and Vegliò [57] used 1-D pseudo-homogeneous model to simulate a side-fired reformer

in a H_2 plant, optimized the tube skin temperature for maximizing the catalytic tube life, and optimum fuel distribution among burners was evaluated to achieve the desired conversion.

The selection of the appropriate catalyst for the reforming process plays a vital role in the overall performance of the SMR process. Although a wide variety of reforming catalysts has been reported by various authors, their performance for SMR applications have not been studied. To fill this gap, in the present work, a 1-D heterogeneous reactor model for SMR developed previously [58] with gPROMS model builder is used to test kinetic data derived from conversion data from this literature review. The predicted results of the reactor model under the various conditions of temperature, pressure, and S/C, were compared with experimental results. To find out the optimum temperature, pressure, S/C, and gas mass flow velocity, a sensitivity analysis of the reactor model was conducted. The predicted results were further compared at equilibrium with results generated through an independent equilibrium-based software.

2. Model Development

A 1-D heterogeneous mathematical reactor model developed in our previous work [58] is employed here to study the performance and behaviour of the SMR process under dynamic and steady-state conditions by considering the transfer of heat and mass in both fluid and solid phases. The reactor model incorporates the mass, heat, and momentum balances as a function of time and axial position along the length of the reactor. The developed model was based on the following assumptions:

a) The flow pattern is assumed to be a non-ideal plug flow.
b) Ideal gas behavior is applicable.
c) The operation is adiabatic in nature.
d) Bed porosity is constant, and the size of the catalyst particles is uniform.
e) Radial variations in concentration and temperature gradient have been neglected i.e. heat and mass flow pattern is only studied in axial direction.
f) The effect of carbon deposition is not considered in this work.

The involvement of several reactions makes SMR a complex process. To minimize the complexity in the model, only those reactions with appreciable kinetic rates and consequently affecting the

overall process were considered. The rate equations for these reactions are given in Appendix A. The mathematical equations for mass, energy, and momentum balances to model the SMR process are given in Table 1.

The inlet and exit boundary conditions to solve the equations of the reactor model are:

At the reactor inlet (z = 0):

$$C_i = C_{i,0}; \quad T = T_0; \quad T_s = T_{s,0}; \quad P = P_0$$

At the reactor outlet (z = L):

$$\frac{\partial C_i}{\partial z} = 0; \quad \frac{\partial T}{\partial z} = 0; \quad \frac{\partial T_s}{\partial z} = 0$$

Initial conditions:

$$C_i = C_{i,0}; \quad T = T_0; \quad T_s = T_{s,0}$$

Table 1: Summary of mass, energy, and momentum balance equations used in the reactor model

Gas phase mass and energy balance:

$$\varepsilon_b\left(\frac{\partial C_i}{\partial t}\right) + \frac{\partial (uC_i)}{\partial z} + k_{g,i}a_v(C_i - C_{i,s}) = \varepsilon_b D_z \frac{\partial^2 C_i}{\partial z^2}$$

$$\varepsilon_b \rho_g C_{pg}\left(\frac{\partial T}{\partial t}\right) + u\rho_g C_{pg}\frac{\partial (T)}{\partial z} = h_f a_v(T_s - T) + \lambda_z^f \frac{\partial^2 T}{\partial z^2}$$

Solid phase mass and energy balance:

$$k_{g,i}a_v(C_i - C_{i,s}) = (1 - \varepsilon_b)\rho_{cat} r_i$$

$$\rho_{bed} C_{p,bed}\left(\frac{\partial T_s}{\partial t}\right) + h_f a_v(T_s - T) = (1 - \varepsilon_b)\rho_{cat}\sum -\Delta H_{rxn,j}\eta_j R_j$$

Pressure drop across the reactor:

$$\frac{\Delta P g_c}{L} = -K_D u - K_V u^2$$

where; $K_D = \frac{150\mu(1-\varepsilon_b)^2}{d_p^2 \varepsilon_b^3}$; $K_V = \frac{1.75(1-\varepsilon_b)\rho_g}{d_p \varepsilon_b^3}$

The equilibrium and kinetic rate constants are presented in Appendix A. The empirical correlations used to determine the physical properties are listed in Appendix B.

Rates for the disappearance and formation of species involved in the reactor system can be written as follows;

$$r_{CH_4} = -\eta_1 R_1 - \eta_3 R_3 \quad (1)$$

$$r_{H_2O} = -\eta_1 R_1 - \eta_2 R_2 - 2\eta_3 R_3 \quad (2)$$

$$r_{CO} = \eta_1 R_1 - \eta_2 R_2 \quad (3)$$

$$r_{H_2} = 3\eta_1 R_1 + \eta_2 R_2 + 4\eta_3 R_3 \quad (4)$$

$$r_{CO_2} = \eta_2 R_2 + \eta_3 R_3 \quad (5)$$

To obtain true reaction kinetics, the size of the catalyst must be selected in such a way that it virtually eliminates the diffusion control limitations. To determine the required size of the particle in which there are no diffusion effects, the Weisz-Prater (WP) criterion can be used [59, 60]

$$CWP = \eta \emptyset_1^2 \quad (6)$$

$$CWP = \frac{-r'_A(obs)\rho_{cat}R_P^2}{D_e C_{A_S}} \quad (7)$$

If CWP << 1, then there are no internal diffusion limitations and ultimately no concentration gradient exists within the catalyst particle. In order to find out how small the size of the particle should be to avoid internal diffusion limitations, the Thiele Modulus (ϕ) and the effectiveness factor (η) need to be calculated. The effectiveness factor is the measure of how far the reactant diffuses into the pellet before reacting. The Thiele modulus and the effectiveness factors are related to each other as;

$$\eta \emptyset_1^2 = 3(\emptyset_1 \coth \emptyset_1 - 1) \quad (8)$$

The reaction rate will be diffusion-limited if the Thiele Modulus ($\emptyset$) is very large, i.e. if $\eta \ll 1$. Intraparticle transport limitations are primarily influenced by the catalyst particle size, while external transport limitations are primarily influenced by the fluid flow velocity. In our present work, we have assumed that the size of the catalyst particles is small enough so that Thiele Modulus ($\emptyset$) is <1, and thus intraporous mass and energy transport resistances are neglected [61], i.e., effectiveness factor (η) is assumed to be unity for all the reactions involved, as already reported for various catalysts and reacting systems [44, 62, 63].

The kinetics for different catalysts available in Table 2, 3 and Table 4 were implemented in our developed model, and the model results were validated and analyzed. CEA, was used to obtain the

equilibrium compositions of species participating in the reforming reactions [64-66], and the results generated were compared with the outputs of the reactor model.

Table 2: Catalyst and catalyst bed properties for various catalysts

Catalyst	Reference	d_p (m)	ρ_{cat} (kg/m^3)	ρ_{bed} (kg/m^3)	ε_b
Catalyst-1	[44]	2.00×10^{-3}	1870	1122	0.4
Catalyst-2	[45]	2.00×10^{-3}	2200	1214	0.448
Catalyst-3	[47]	1.50×10^{-4}	2797	1566	0.44
Catalyst-4	[67]	1.75×10^{-3}	3737	2429	0.35
Catalyst-5	[68]	5.60×10^{-3}	1687	877	0.48
Catalyst-6	[69]	1.60×10^{-3}	1274	726	0.43
Catalyst-7	[70]	3.00×10^{-4}	15.9	9.54	0.4
Catalyst-8	[71]	2.15×10^{-4}	2200	1320	0.4
Catalyst-9	[72]	2.00×10^{-3}	1870	1122	0.4
Catalyst-10	[72]	2.00×10^{-3}	1870	1122	0.4
Catalyst-11	[58]	1.20×10^{-3}	1870	1122	0.4
Catalyst-12	[43]	5.4×10^{-3}	2355	1154	0.51

Table 3: Arrhenius kinetic parameters of various catalysts

Catalyst	E_1 (J/mol)	E_2 (J/mol)	E_3 (J/mol)	$k_{o,1}$ (mol/(kg$_{cat}$ s))	$k_{o,2}$ (mol/(kg$_{cat}$ s))	$k_{o,3}$ (mol/(kg$_{cat}$ s))
Catalyst-1	240,100	67,130	243,900	1.17×10^{15} bar$^{0.5}$	5.43×10^{5} bar^{-1}	2.83×10^{14} bar$^{0.5}$
Catalyst-2	-	32,520	185,592	-	4.08×10^{4} bar^{-1}	1.19×10^{12} bar$^{0.5}$
Catalyst-3	209,200	15,400	109,400	1.87×10^{11} bar$^{0.25}$	6.03×10^{-3} bar	3.46×10^{5} bar$^{0.25}$
Catalyst-4	209,500	70,200	211,500	9.048×10^{11} bar$^{0.5}$	5.43×10^{5} bar^{-1}	2.14×10^{9} bar$^{0.5}$
Catalyst-5	218,550	73,523	236,850	5.83×10^{11} bar$^{0.5}$	2.51×10^{4} bar^{-1}	4.67×10^{13} bar$^{0.5}$
Catalyst-6	217,010	68,200	215,840	5.79×10^{12} bar$^{0.5}$	9.33×10^{6} bar^{-1}	1.29×10^{13} bar$^{0.5}$
Catalyst-7	83,800	15,100	89,200	1.62×10^{7} bar$^{0.5}$	2.34×10^{7} bar^{-1}	4.55×10^{7} bar$^{0.5}$

Catalyst-8	216,722	67,966	227,941	9.78×10^{14} $bar^{0.5}$	5.29×10^{5} bar^{-1}	2.57×10^{14} $bar^{0.5}$
Catalyst-9	240,100	-	209,754	4.13×10^{13} $bar^{0.5}$	-	8.29×10^{11} $bar^{0.5}$
Catalyst-10	247,303	-	265,851	4.88×10^{14} $bar^{0.5}$	-	1.17×10^{15} $bar^{0.5}$
Catalyst-11	257,010	89,230	236,700	5.19×10^{12} $bar^{0.5}$	9.90×10^{6} bar^{-1}	1.32×10^{13} $bar^{0.5}$
Catalyst-12	106780	54531	-	2.62×10^{5} $bar^{0.404}$	2.45×10^{2} bar^{-1}	-

Table 4: Van't Hoff adsorption parameters of species CH_4, CO, H_2, H_2O, and CO_2

Catalysts	$\mathbf{K_{o,CH_4}\ (bar)^{-1}}$	$\mathbf{K_{o,CO}\ (bar)^{-1}}$	$\mathbf{K_{o,H_2}\ (bar)^{-1}}$	$\mathbf{K_{o,H_2O}\ (bar)^{-1}}$	$\mathbf{K_{o,CO_2}\ (bar)^{-1}}$	$\mathbf{\Delta H_{CH_4}\ (J/mol)}$	$\mathbf{\Delta H_{CO}\ (J/mol)}$	$\mathbf{\Delta H_{H_2}\ (J/mol)}$	$\mathbf{\Delta H_{H_2O}\ (J/mol)}$	$\mathbf{\Delta H_{CO_2}\ (J/mol)}$
Catalyst-1	6.65×10^{-4}	8.23×10^{-5}	6.12×10^{-9}	1.77×10^{5} bar	-	-38,280	-70,650	-82,900	88,680	-
Catalyst-2	-	2.90	-	6×10^{4} bar	-	-	-19,813	-	54,340	-
Catalyst-3	-	5.13×10^{-11}	5.68×10^{-9} $(bar)^{0.5}$	9.25 bar	-	-	-140,000	-93,400	15,900	-
Catalyst-4	1.995×10^{-3}	8.11×10^{-5}	7.05×10^{-9}	1.68×10^{4} bar	-	-36,650	-70,230	-82,550	85,770	-
Catalyst-5	6.65×10^{-4}	8.23×10^{-5}	6.12×10^{-9}	1.77×10^{5} bar	-	-38,280	-70,650	-82,900	88,680	-
Catalyst-6	6.65×10^{-4}	8.23×10^{-5}	6.12×10^{-9}	1.77×10^{5} bar	-	-38,280	-70,650	-82,900	88,680	-
Catalyst-7	1.49×10^{-6}	2.34×10^{-6}	3.88×10^{-5}	2.91×10^{8} bar	8.33×10^{-8}	-98,800	-111,200	-88,200	112,300	-115,600
Catalyst-8	9.58×10^{-4}	8.09×10^{-5}	6.20×10^{-9}	1.68×10^{5} bar	-	35,773	-70,187	-82,643	87,743	-
Catalyst-9	1.09×10^{-3}	-	-	1.04×10^{6} bar	-	-34,835	-	-	98,435	-
Catalyst-10	2.82×10^{-4}	-	-	1.23×10^{6} bar	-	-44,022	-	-	100,208	-
Catalyst-11	6.65×10^{-4}	8.23×10^{-5}	6.12×10^{-9}	1.77×10^{5} bar	-	-38,280	-70,650	-82,900	88,680	-
Catalyst-12	6.65×10^{-4}	8.23×10^{-5}	6.12×10^{-9}	1.77×10^{5} bar	-	-38,280	-70,650	-82,900	88,680	-

3. Thermodynamic analysis of SMR

The optimal operating conditions for the SMR process can be obtained by performing a sensitivity analysis that considers all the variables affecting the performance of the SMR process. Although Xu and Froment [44] explained that the global reaction (R3) is also necessary to represent the experimental kinetic rate data, this work considered that reaction R1 and R2 are sufficient to illustrate the thermodynamic equilibrium of the SMR process [73].

A substantial number of studies have been published describing the thermodynamic analysis of the SMR process [74-76]. The Gibbs free energy minimization and entropy maximization methods can be used to determine the equilibrium product distribution and equilibrium temperature, respectively [74]. In this work, our previously developed model [58] was first simulated by using the widely accepted kinetic model of Xu and Froment [44] and employing the same catalyst over which these kinetics were developed by the authors. Equilibrium conditions were used to perform the thermodynamic analysis and for the model validation against equilibrium data obtained from CEA software. In order to carry out the thermodynamic analysis, the gaseous species CH_4, CO, H_2, H_2O, CO_2 and N_2 were considered in the reaction mixture. To examine the effect of temperature, both pressure and ratio of feedstock were fixed. The effect of pressure was investigated by keeping the temperature and feedstock ratio at a constant value. Similarly, the effect of S/C on the performance of SMR was investigated at a fixed temperature and pressure. The following equations were used to calculate the fuel conversion, H_2 yield (wt. % of feed CH_4) and purity:

$$\mathrm{CH_4\ Conversion\ [\%]} = \frac{(n_{CH4.in} - n_{CH4,out})}{n_{CH4,in}} \times 100 \tag{9}$$

$$\mathrm{H_2\ Purity\ [\%]} = \frac{n_{H2,out}}{(n_{H2,out} + n_{CH4,out} + n_{CO,out} + n_{CO2,out})} \times 100 \tag{10}$$

$$\mathrm{H_2\ Yield\ [wt.\%\ of\ CH_4]} = \frac{(\mathrm{mol.\ weight\ of\ H_2} \times n_{H2,out})}{(\mathrm{mol.\ weight\ of\ CH_4} \times n_{CH4,in})} \times 100 \tag{11}$$

3.1 Effect of temperature, pressure and S/C

Temperature plays an important role towards the sensitivity of the SMR process. At equilibrium, when the reactor is stimulated by an increase in temperature, a rise of the rate of the SMR reaction (R1) (according to Le Chatelier's principle) is observed. In Fig. 1(a-b), the effect of temperature on feed conversion, H_2 yield (wt. % of CH_4), and H_2 purity is shown. The mean relative error, between the results of the proposed model and the results generated using CEA, was 1.95%, which demonstrated a good correlation. It can be observed from Fig. 1(a) that the temperature has a positive effect on CH_4 conversion. The effect of temperature on H_2 yield and purity is exhibited in Fig. 1(b). The results show that the H_2 purity increases as the temperature rises from 673 to 1023 K, but beyond 1023 K, a minor drop in H_2 purity is recorded. This H_2 purity decline is produced as a result of the reverse R2, although CH_4 conversion remains still maximum at such high temperatures. It is evident from Fig. 1(b) that H_2 yield grows rapidly in the temperature interval of 673 – 923 K and attains a value of 42% at 923 K, whilst from 1073 – 1273 K, the H_2 yield does not vary substantially and lastly drops down to 40.8% at 1273 K.

To investigate the effect of pressure on feed (CH_4 and H_2O) conversion, H_2 yield and purity, a temperature condition of 973 K and S/C of 3.0 is used. Fig. 2(a) shows that the low pressure favors the CH_4 conversion. The high pressure shifts the equilibrium towards reactants in the SMR reaction because of having a larger number of moles on the product side, which in turn, results in low CH_4 conversion. In Fig. 2(b), the effect of pressure on H_2 purity and H_2 yield is presented. The results displayed reveal that H_2 yield (wt. % of CH_4) and purity, both decrease with an increase in pressure.

The choice of an optimum S/C is of paramount importance owing to its effect on the overall performance of the SMR process. Higher S/C, which tends to shift R1 in the forward direction, results in improved production of H_2 as a result of an increase in overall conversion of CH_4. A comparison between modelling and equilibrium results is presented in Table 4.

Carbon deposition is an inevitable phenomenon in H_2 production and it occurs in all catalytic transformations of hydrocarbons and can cause catalyst deactivation and hence the involved costs are massive [77]. There are two principal coke formation pathways for steam reforming of methane: the methane dissociation (R6) and disproportionation of CO by exothermic Boudouard reaction (R7) which is favored by a lack of hydrogen [78, 79].

$$CH_{4(g)} \rightleftharpoons C_{(s)} + 2H_{2(g)} \qquad \Delta H_{rxn,298K} = 75\ kJ\ mol_{CH_4}{}^{-1} \tag{R6}$$

$$2CO_{(g)} \rightleftharpoons CO_{2(g)} + C_{(s)} \qquad \Delta H_{rxn,298K} = -172.5\ kJ\ mol_{CO}{}^{-1} \tag{R7}$$

The most common type of carbon deposition is called whisker carbon and during SMR it occurs on the surface of the Ni catalyst. In addition, there are carbon deposits in which carbon is generated as a core of the feedstock radical called encapsulating polymers. This phenomenon is observed as the activity of the catalyst gradually decreases. The third carbon deposition is called pyrolytic carbon, which is generated by the thermal decomposition of hydrocarbons as a feedstock [80]. Many researchers have studied the carbon formation on catalysts, which may be influenced directly by catalyst manufacture [81-84]. The coke resistance of the Ni-based catalysts can be escalated by enhancing the adsorption of steam or CO_2, by increasing the rate of the surface reaction, or by decreasing the rate and degree of methane activation and dissociation [79]. This can be achieved by the use of promoters and several reports of alkali or alkaline earth metal promoted catalysts in the literature have been outlined by Hu and Ruckenstein [85]. The inhibition of carbon formation can be promoted if CO_2 adsorption is enhanced and this can be done by using Ni catalysts that incorporate basic metal oxides [86, 87]. The anti-coke formation performance can be significantly improved if the catalyst possesses a strong interaction between nickel and the support or if the Ni precursor is located within a well-defined structure. Many recent attempts have been made to confine Ni particles in nickel precursors with defined structures and with such structures, high dispersion of the metal could be achieved with enhanced coke resistance for reforming reactions [88-91]. As discussed, catalyst preparation is of paramount importance, and most of the reported studies employed conventional catalyst preparation methods, like impregnation or sol–gel, followed by calcination and thermal reduction. However, some new preparation methods have been exploited for the preparation of Ni-based catalysts and methods include combustion, microwave radiation, supercritical, plasma treatment. The catalysts prepared this way evinces a high activity and exhibit fuel conversion close to the predicted by thermodynamic calculations [92-97].

Usually, in a reformer, carbon deposition often occurs on the inlet side of the catalyst layer, and most of it is whisker carbon. The cause is considered to be due to low S/C at the start of the reformer, and when carbon is generated, it cannot be removed, and thus the reformer has to be

replaced. Therefore, preventing the formation of unreactive carbon deposits in the first place is of great importance [98]. The probability of carbon deposition depends not only on the partial pressures of the reactants but also on the catalyst composition and the process conditions. Principally, the problem of carbon deposition is a competition between deposition and reforming. When the rate of reforming outbalances the rate of deposition, catalyst deactivation due to carbon deposition is prevented [99]. Thus, excess steam not only favors the CH_4 conversion but also enhances the production of H_2 and reduces the possibility of coke deposition on the surface of the catalyst. According to the results, high CH_4 conversion, H_2 yield (wt. % of CH_4), and purity can be obtained by using steam in excess although this would impact on the overall operational cost of the process. Therefore, the optimum S/C is always a compromise between the overall efficiency and operational cost.

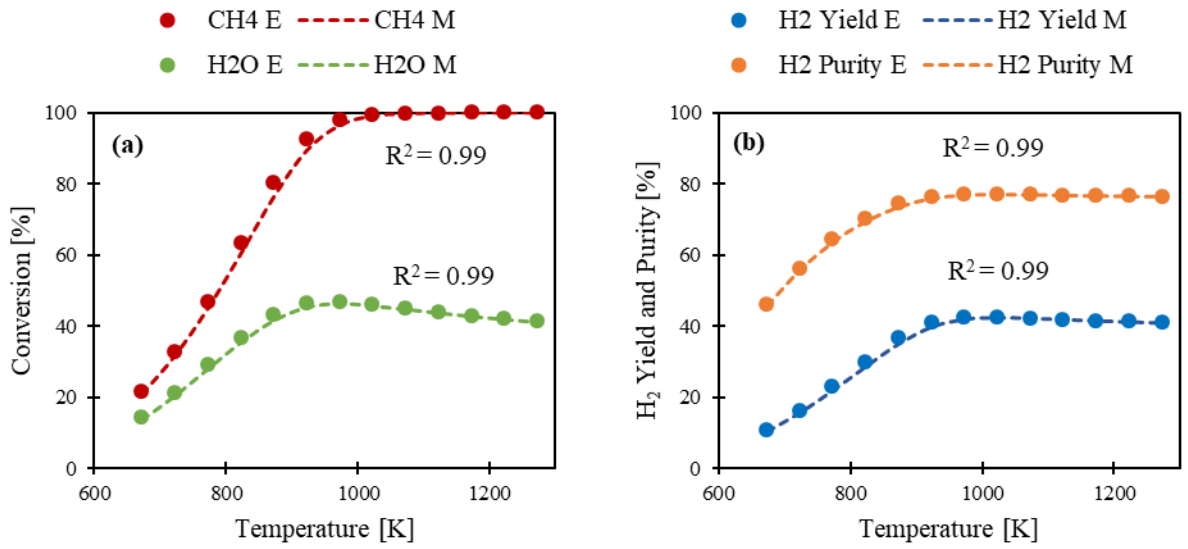

Fig. 1. Effect of the temperature on a) CH_4 and H_2O conversion; b) H_2 yield (wt. % of CH_4) and H_2 purity at 1 bar and S/C of 3.0 (**E:** Equilibrium and **M:** Modelling).

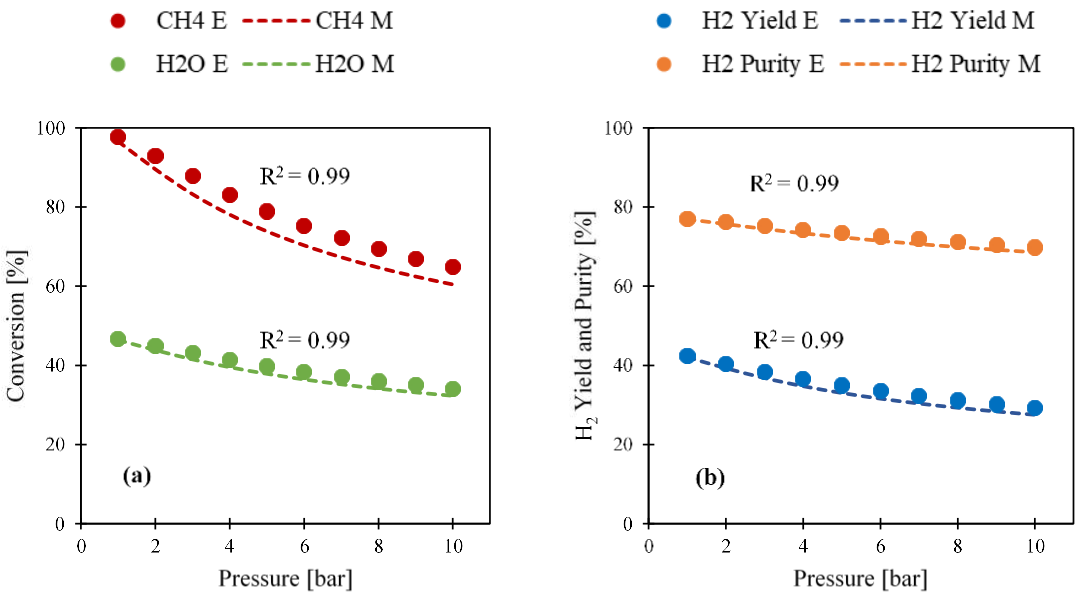

Fig. 2. Effect of pressure on a) CH_4 and H_2O conversion; b) H_2 yield (wt. % of CH_4) and H_2 purity at 973 K and S/C of 3.0 (**E:** Equilibrium and **M:** Modelling).

Table 5: Effect of S/C on CH_4 conversion, H_2 yield (wt. % of CH_4) and H_2 purity at 973 K and 1 bar (E: Equilibrium and M: Modelling)

S/C	**CH_4 Conversion [%]**	**H_2 Yield [wt. % of CH_4]**	**H_2 Purity [%]**
1	M: 71.7 E: 76.8	M: 28.3 E: 30.0	M: 69.2 E: 70.4
2	M: 90.9 E: 94.1	M: 38.0 E: 39.1	M: 75.1 E: 75.6
3	M: 96.6 E: 97.8	M: 42.0 E: 42.4	M: 76.9 E: 77.1
4	M: 98.5 E: 99.0	M: 44.1 E: 44.2	M: 77.7 E: 77.8
5	M: 99.3 E: 99.5	M: 45.3 E: 45.3	M: 78.2 E: 78.2
6	M: 99.6 E: 99.7	M: 46.1 E: 46.0	M: 78.5 E: 78.5

4. Model validation of SMR using industrial conditions

After validating the reactor model with equilibrium data, validation is conducted with steady-state industrial data. Non-equilibrium conditions of industrial settings are represented by the gas mass flow velocity G_s. G_s of 3.5 kg m^{-2} s^{-1} is used, producing results close to, but not at equilibrium. Table 6 shows the comparison of outputs obtained from the proposed reactor model with literature data [100] and a mean relative error of 5.9% is found, showing that the model outputs are in good agreement with the literature results. The predicted results of the outlet molar composition of the reforming product gases are compared with the industrial data [53] presented in Table 7. Table 7 allied with Fig. 3 confirms that the simulation results are in excellent agreement with industrial data.

Table 6: Comparison of literature data [100] with predicted results in terms of molar fraction of the product gases at the outlet of the reactor for a temperature range of 773 – 1273 K, 10 bar, and S/C of 2.0.

Operating Conditions	**Components**	**Molar fraction of the product gases at the reactor outlet**											
		773 K		**873 K**		**973 K**		**1073 K**		**1173 K**		**1273 K**	
		This work	**[100]**	**This work**	**[100]**	**This work**	**[100]**	**This work**	**[100]**	**This work**	**[100]**	**This work**	**[100]**
P = 10 atm S/C = 2.0	CH_4	0.263	0.260	0.209	0.203	0.142	0.126	0.075	0.050	0.028	0.015	0.007	0.004
	CO	0.002	0.004	0.014	0.015	0.049	0.061	0.101	0.115	0.145	0.153	0.168	0.168
	H_2	0.167	0.174	0.285	0.300	0.410	0.434	0.518	0.563	0.588	0.610	0.615	0.625
	H_2O	0.528	0.524	0.432	0.421	0.334	0.314	0.252	0.222	0.201	0.184	0.182	0.176
	CO_2	0.040	0.038	0.060	0.061	0.065	0.065	0.053	0.050	0.038	0.038	0.028	0.027

Table 7: SMR industrial operating conditions adopted from the literature [53].

Pressure [P]	29 bar
Gas feed temperature [T]	760 °C
Catalyst temperature [T_s]	760 °C
Inlet mole fractions	
CH_4	0.2128
H_2	0.0260
H_2O	0.7144
CO_2	0.0119
N_2	0.0350

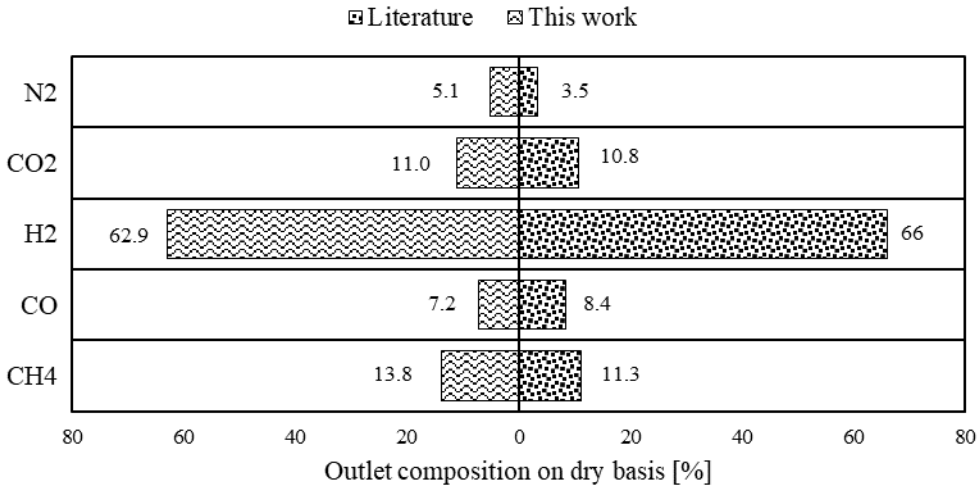

Fig. 3. Comparison of molar composition of the product gases (dry basis) at the outlet of reactor obtained via simulated results with literature data under the operating conditions tabulated in Table 7.

4.1 Effect of G_s

The gas mass flow velocity (G_s) is one of the most important operating parameters that affect the performance of the SMR process. The selection of the optimum G_s depends on the length and loading of the reformer. To obtain the CH_4 conversion near an equilibrium value, a velocity of 1.5 - 2 m s^{-1} is used [101]. The performance of the SMR process is evaluated with various values of

G_s using the Xu and Froment [44] kinetic model over Ni/$MgAl_2O_4$ catalyst.

In Fig. 4, the dynamic variation of H_2 and CH_4 composition (dry basis) at the outlet of the reactor under the fixed operating conditions of 973 K, 30 bar, S/C of 3, and various G_s (1 – 5 kg $m^{-2}s^{-1}$) is presented. The low G_s produce longer residence times and a CH_4 conversion closer to the equilibrium value is achieved. For a G_s of 1 kg $m^{-2}s^{-1}$, the conversion of CH_4 is 43.7%, which is comparable to the equilibrium value of 44.3% under the same operating conditions. For higher G_s values, a decrease in CH_4 conversion is observed because of the lower residence time throughout the reactor. The G_s value of 3.5 kg $m^{-2}s^{-1}$ produces a CH_4 conversion and H_2 purity of 41.5% and 60.7%, respectively corresponding to 44.3% and 62.1% at equilibrium. Therefore, a G_s of 3.5 kg $m^{-2}s^{-1}$ is opted because, at this value, a high CH_4 conversion is maintained.

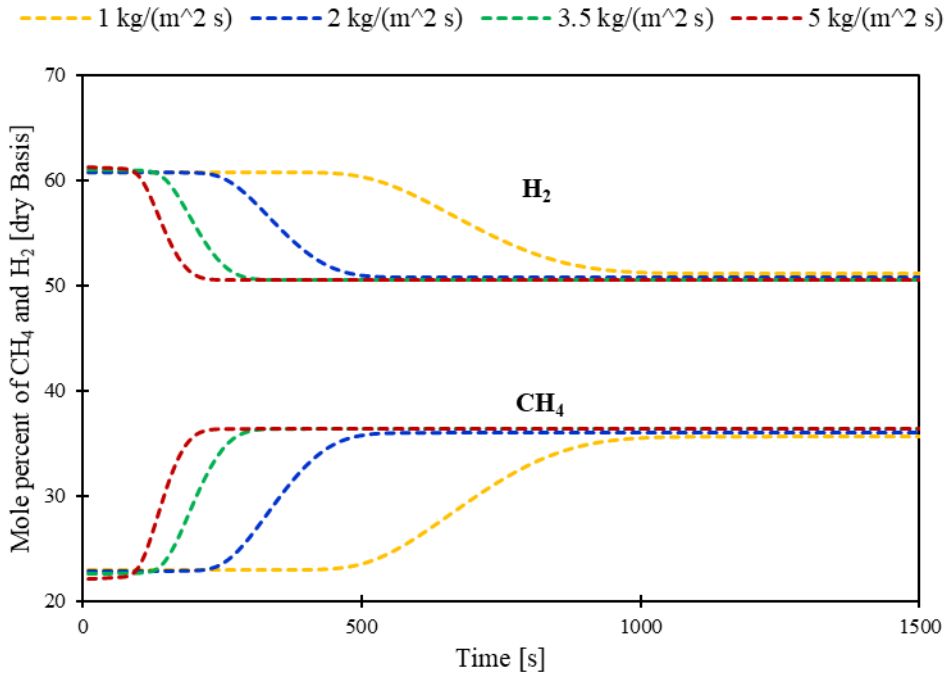

Fig. 4. Dynamic profile of CH_4 and H_2 composition (dry basis) at the exit of the reactor for various G_s values at 973 K, 30 bar, and S/C of 3.0.

5. Performance of SMR process over various catalysts

After the validation of the developed reactor model, the performance of the SMR process is predicted by implementing the kinetics data available in the literature on the developed reactor

model. For this purpose, a set of 12 different catalysts with available kinetics is selected. Xu and Froment [44], using a commercial 15 wt. % Ni catalyst supported on magnesium spinel (Catalyst-1), developed a general intrinsic kinetic model. The rate equations are given in Appendix A (A.1 - A.4). Soliman et al. [45] studied the intrinsic kinetics of SMR over a Ni/calcium aluminate catalyst (Catalyst-2). Hou and Hughes [47] developed a kinetic model by using a commercial Ni/Al_2O_3 catalyst with NiO content of 15 – 17 wt. % (Catalyst-3). The rate equations are given in Appendix A (A.5 - A.8). Hoang et al. [67] determined the kinetics of SMR over a Ni sulfide catalyst with 9.8% Ni on a gamma-alumina support (Catalyst-4). Oliveira et al. [68, 69] determined the true kinetics of SMR over commercial Ni/Al_2O_3 catalyst (Catalyst-5) and a pre-commercial Ni/Al_2O_3 catalyst (Catalyst-6) with 15.4 and 10% Ni content, respectively.

Halabi et al. [70] used $Rh/Ce_{0.6}Zr_{0.4}O_2$ (Catalyst-7) in an integral fixed-bed reactor to determine the true kinetics of SMR. The rate equations are shown in Appendix A (A.9 - A13). The kinetics of SMR over the 10.34 wt. % Ni/Al_2O_3 (Catalyst-8) sample were determined in an adiabatic fixed-bed reactor by Kanhari et al. [71]. Obradović et al. [72] predicted the intrinsic kinetic of SMR on commercial 11.8 wt. % Ni-based catalyst (Catalyst-9) and on commercial $Pt/Ni/Al_2O_3$ (Catalyst-10). Abbas et al. [58] studied the kinetics of SMR over an 18 wt. % $NiO/\alpha\text{-}Al_2O_3$ commercial catalyst (Catalyst-11). Numaguchi and Kikuchi [43] determind the kinetics of SMR in an integral flow reactor using a Ni-based catalyst with 8.7 wt. % Ni content (Catalyst-12) and the rate equations are given in Appendix A(A.19 - A.20).

5.1 Comparison in terms of CH_4 conversion, H_2 yield (wt. % of CH_4) and H_2 purity

As seen in section 4.1, the G_s value plays an important role to achieve equilibrium conditions. In this section, performance in terms of CH_4 conversion, H_2 yield (wt. % of CH_4), and H_2 purity at conditions away from the equilibrium is studied. After successful validation of the model, here comparison of performance of chosen catalysts will be carried out under medium-high pressure corresponding to industrial SMR conditions. In Fig. 5 (a), the conversion of CH_4 at the exit of the reformer of various catalysts (catalyst 1 – 12) predicted under the operating conditions of 973 K, 30 bar, and S/C of 3.0, is presented. Simulations with catalyst – 8, which is a Ni-based catalyst, generated the highest CH_4 conversion of 42% that was favoured by its very fast kinetics, close to the equilibrium predicted value of 44.3%.

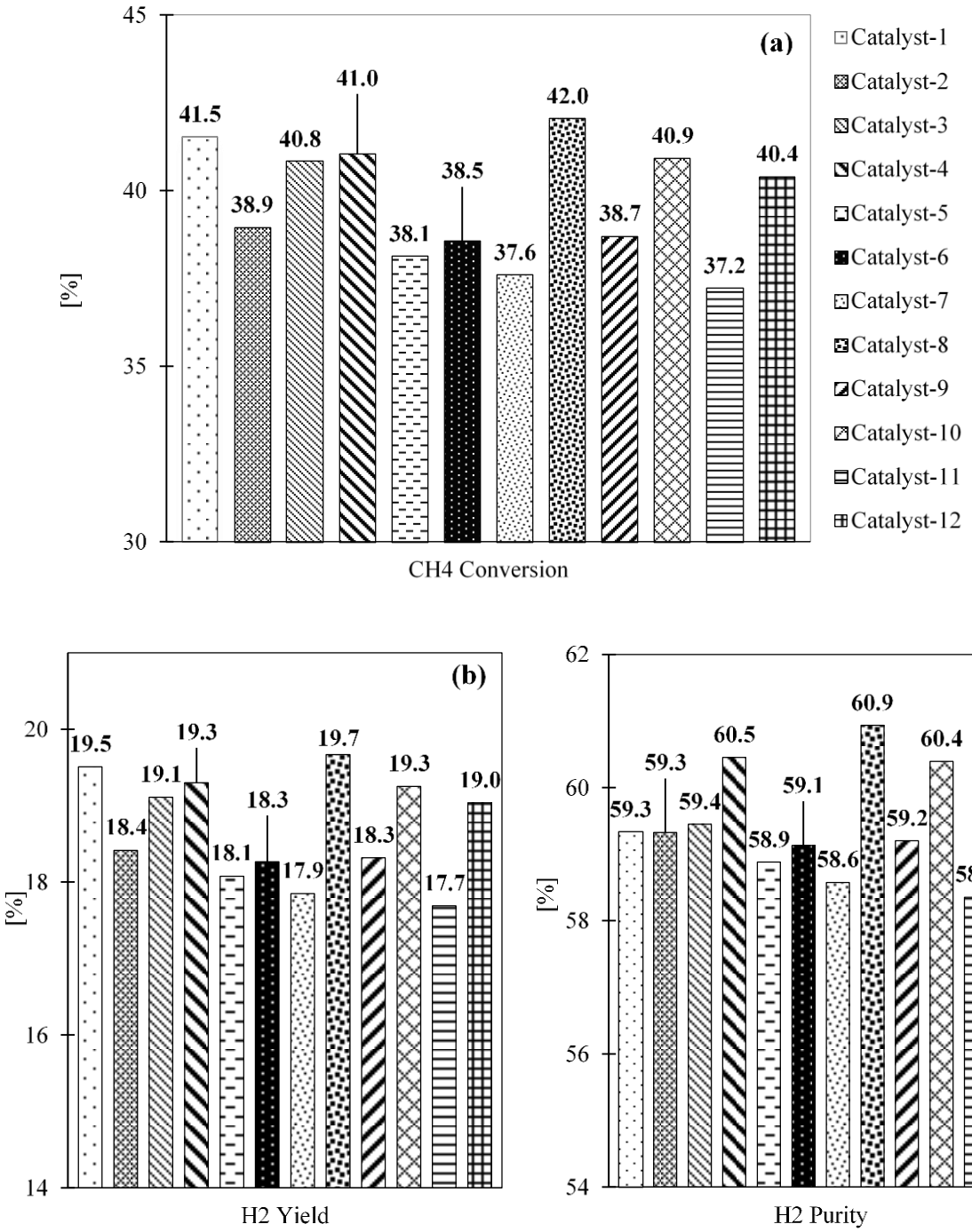

Fig. 5. Comparison in terms of a) CH_4 conversion; b) H_2 yield (wt. % of CH_4); c) H_2 purity over various catalysts at 973 K, 30 bar, S/C of 3.0 and G_s of 3.5 kg $m^{-2}s^{-1}$. Equilibrium values were 44.3% for CH_4 conversion, 20.6% for H_2 yield, and 62% for H_2 purity.

The activation energy for R1, using catalyst - 8, is low, and thus, the value of the rate constant is high. Therefore, the rate of disappearance of CH_4 is much higher for catalyst - 8 compared to the

other catalysts used in the present work. Fig. 5(b) shows the H_2 yield (wt. % of feed CH_4) during SMR process using various catalysts. The catalyst - 8 gives 10.2% more H_2 yield than catalyst – 11 under the same operating conditions of 973 K, 30 bar, and S/C of 3.0. Fig. 5(c) indicates that there is no abrupt variation in the H_2 purity as a result of swapping the catalyst. Fig. 6 features the dynamic profile of the rate of the SMR reaction (R1), of various catalysts at the exit of the reactor under the operating conditions of 973 K, 30 bar, S/C of 3.0, and G_s of 3.5 kg $m^{-2}s^{-1}$. The highest value for the rate of the SMR reaction is observed when the reformer is loaded with the catalyst – 8 contributing to the highest CH_4 conversion amongst all the studied catalysts (Fig. 5(a)). The following catalyst activity order is observed in terms of CH_4 conversion: catalyst-8 > catalyst-1 > catalyst-4 > catalyst-10 > catalyst-12 > catalyst-3 > catalyst-2 > catalyst-9 > catalyst-6 > catalyst-5 > catalyst-7 > catalyst-11. Catalyst-11 shows the lowest CH_4 conversion (37.2%) compared to the other catalysts. According to the mechanism proposed by Soliman et al. [45], the rate of R1 is zero for the catalyst-2, and the CO_2 produced during R3 is converted to CO by reverse R2.

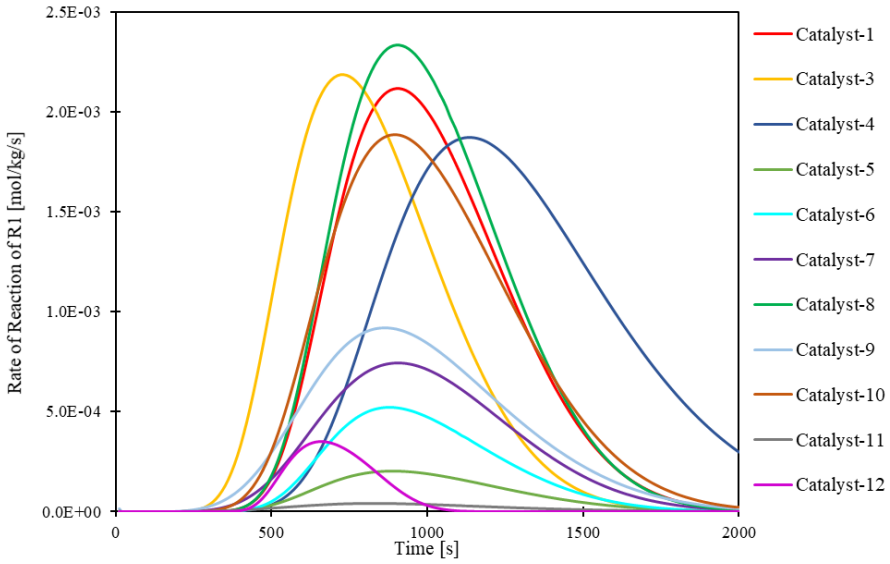

Fig. 6. The dynamics profile of the rate of the SMR reaction R1 at the exit of the reactor of various catalysts studied at 973 K, 30 bar, S/C 3.0 and G_s of 3.5 kg $m^{-2}s^{-1}$.

Fig. 7 shows the variation of gas temperature at the exit of the reactor under the operating conditions of 973 K feed temperature, 30 bar, S/C of 3.0, and G_s of 3.5 kg $m^{-2}s^{-1}$. The SMR process is highly endothermic and the reactor is operated under adiabatic conditions. In a first instance, the feed is introduced at 973 K (Fig. 7), and subsequently at 1173 K (Fig. 8) to illustrate the effect of temperature on the reforming kinetics of the different catalysts. It can be observed in Fig. 7 that

there is no rapid change in temperature of the gas before 750s for almost all catalysts under analysis, but after 750s, there is a sudden decline in the gas temperature because of the endothermic SMR (R1). For the period beyond 1500 s, the gas temperature for catalyst - 8 is 907 K showing a drop of 66 K, which indicates governance of R1.

The choice of 973 K for a pressure of 30 bar is on the lower side for industrial conditions and some catalysts' kinetics may overtake others at higher temperatures. Fig. 8 (a-c) shows the comparison between different reforming catalysts in terms of CH_4 conversion, H_2 yield (wt. % of CH_4), and H_2 purity at a temperature of 1173 K and 30 bar. It is evident from Fig. 8(a) that catalyst - 3 exhibits a 112% increase in CH_4 conversion as temperature varies from 973 K to 1173 K and at 86.4%, it attains the highest amongst all catalysts, closest to the equilibrium conversion of 88.6%. It can be seen from Fig. 8(b) that the maximum increase in H_2 yield is observed for catalyst - 11, but due to the fast kinetics at elevated temperatures, catalyst - 3 provides a yield of 36.9% in comparison to an equilibrium yield of 37.2%. The catalyst-11 displays maximum improvement in its performance in comparison to all other catalysts at high temperature but catalyst - 3 still proves itself the better amongst all in terms of H_2 purity also. The catalyst - 3 gives a H_2 purity of 74.4% (Fig. 8(c)) which is close to the equilibrium purity value of 74.6% under identical operating conditions of temperature, pressure, and fuel to steam ratio.

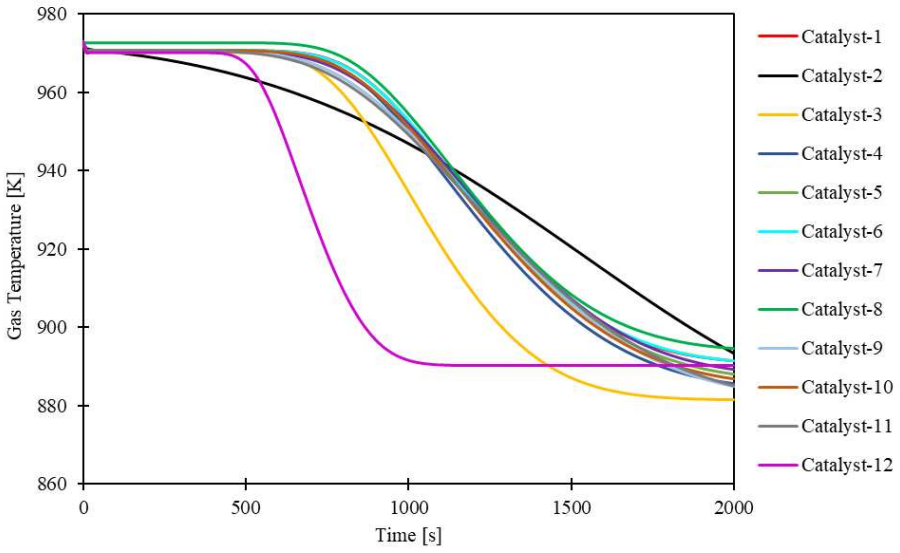

Fig. 7. The dynamic profile of the gas temperature over various catalysts at 973 K feed temperature, 30 bar, S/C 3.0, and G_s of 3.5 kg $m^{-2}s^{-1}$.

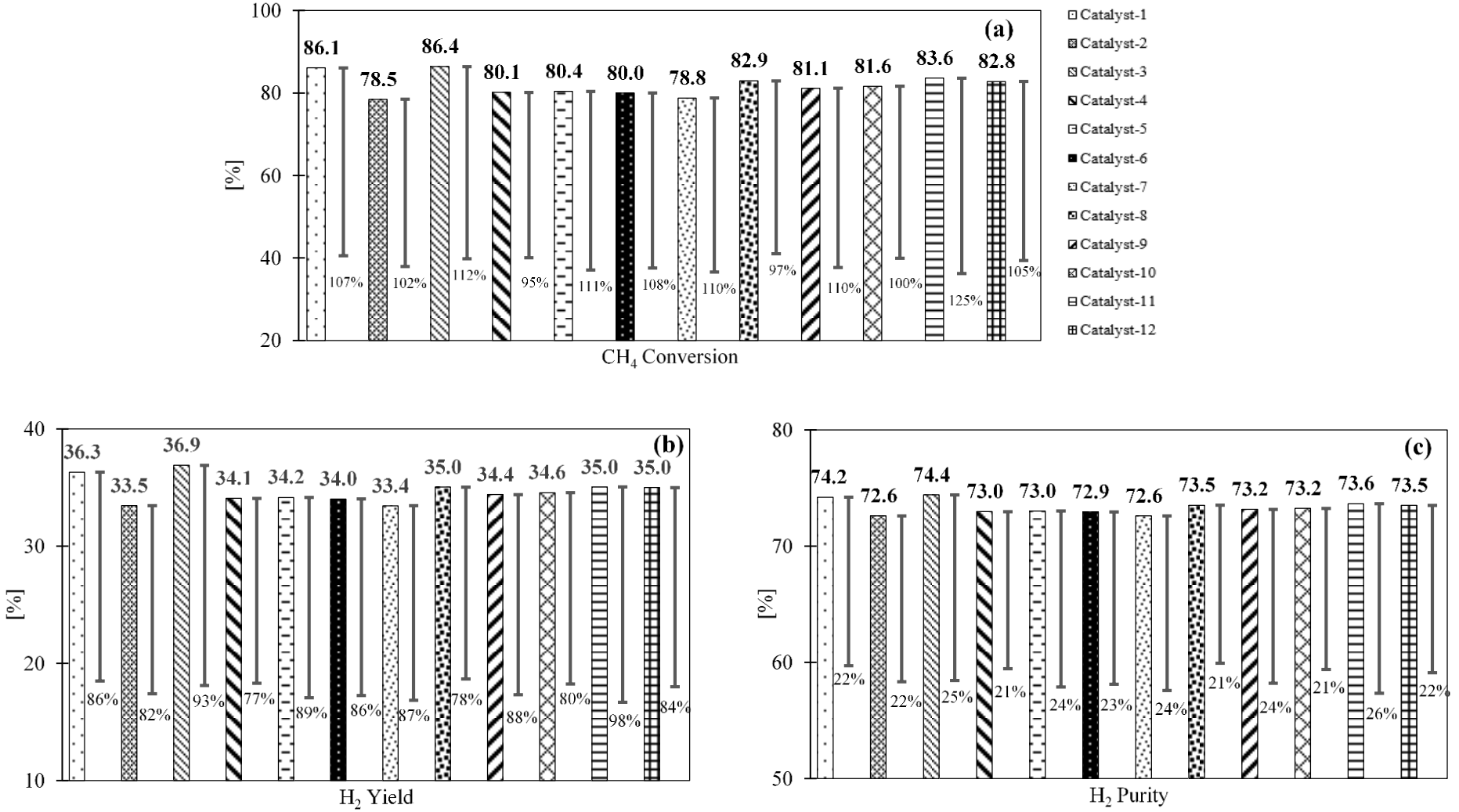

Fig. 8. Comparison between different catalysts in terms of a) CH_4 conversion; b) H_2 yield (wt. % of CH_4); c) H_2 purity over various catalysts at 1173 K, 30 bar, S/C of 3.0 and G_s of 3.5 kg $m^{-2}s^{-1}$. Equilibrium values were 88.6% for CH_4 conversion, 37.2% for H_2 yield, and 74.6% for H_2 purity. The % bars next to the pattern bars are in order from left to right (Catalyst-1 to Catalyst-12) and they represent the % increase or decrease when the temperature is increased from 973 K to 1173 K.

5.2 Selectivity of C-based and H-based products

The selectivity of C-based and H-based products in effluent gases is modelled using the following equations;

$$\text{CO Selectivity (\%)} = \frac{\dot{n}_{CO}}{\left(\dot{n}_{CH_4} + \dot{n}_{CO} + \dot{n}_{CO_2}\right)} \times 100 \quad (12)$$

$$\text{CO}_2\text{ Selectivity (\%)} = \frac{\dot{n}_{CO_2}}{\left(\dot{n}_{CH_4} + \dot{n}_{CO} + \dot{n}_{CO_2}\right)} \times 100 \quad (13)$$

$$\text{H}_2\text{ Selectivity (\%)} = \frac{\dot{n}_{H_2}}{\left(\dot{n}_{CH_4} + \dot{n}_{H_2}\right)} \times 100 \quad (14)$$

Where, $\dot{n}_{CH_4}$, $\dot{n}_{CO}$, $\dot{n}_{CO_2}$ and $\dot{n}_{H_2}$ correspond to the molar flowrates of CH_4, CO, CO_2 and H_2 at the outlet of the reactor.

Fig. 9 (a-b) shows for 973 K feed temperature and 30 bar reformer pressure, the catalysts comparison in terms of selectivity of C-based products, and Fig. 9 (c) depicts the selectivity of H_2, when the reformer is allowed to run with identical operating conditions but loaded with different catalyst. In Fig. 9(a), the selectivity of CO is maximum for catalyst-8 compared to the other catalysts due to the maximum rate of disappearance for CH_4. Catalyst-3 gives the maximum CO_2 selectivity (29.9%) as is displayed in panel (b) of Fig. 9. This high value of selectivity suggests that CO_2 is the primary product using the catalyst-3, which is then converted to CO via reverse R2. In Fig. 9(c), the selectivity of H_2 is the highest (72.9%) using catalyst-8, while the catalyst-11 shows a value of 69.1 % for H_2 selectivity under comparable operational conditions of 973 K, 30 bar and S/C of 3.0. The results indicate that the selectivity of carbon-containing products strongly depends on the thermodynamics of reactions. Thus, the reaction kinetics dictate the primary product.

Similar to Fig. 9, Fig. 10 (a-c) shows the selectivity of C-based and H-based products, but at a feed temperature of 1173 K. The maximum increase in CO selectivity is observed for catalyst-3 and catalyst-11 (Fig. 10(a)) while there is no appreciable change in CO_2 selectivity (Fig. 10(b)) for any other catalyst when temperature is increased from 973 K to 1173 K. It can be observed from Fig. 10(c) that the maximum H_2 selectivity is associated with the catalyst-3 supplying a H_2 selectivity of 95.4% while equilibrium would provide a selectivity of 96.3%.

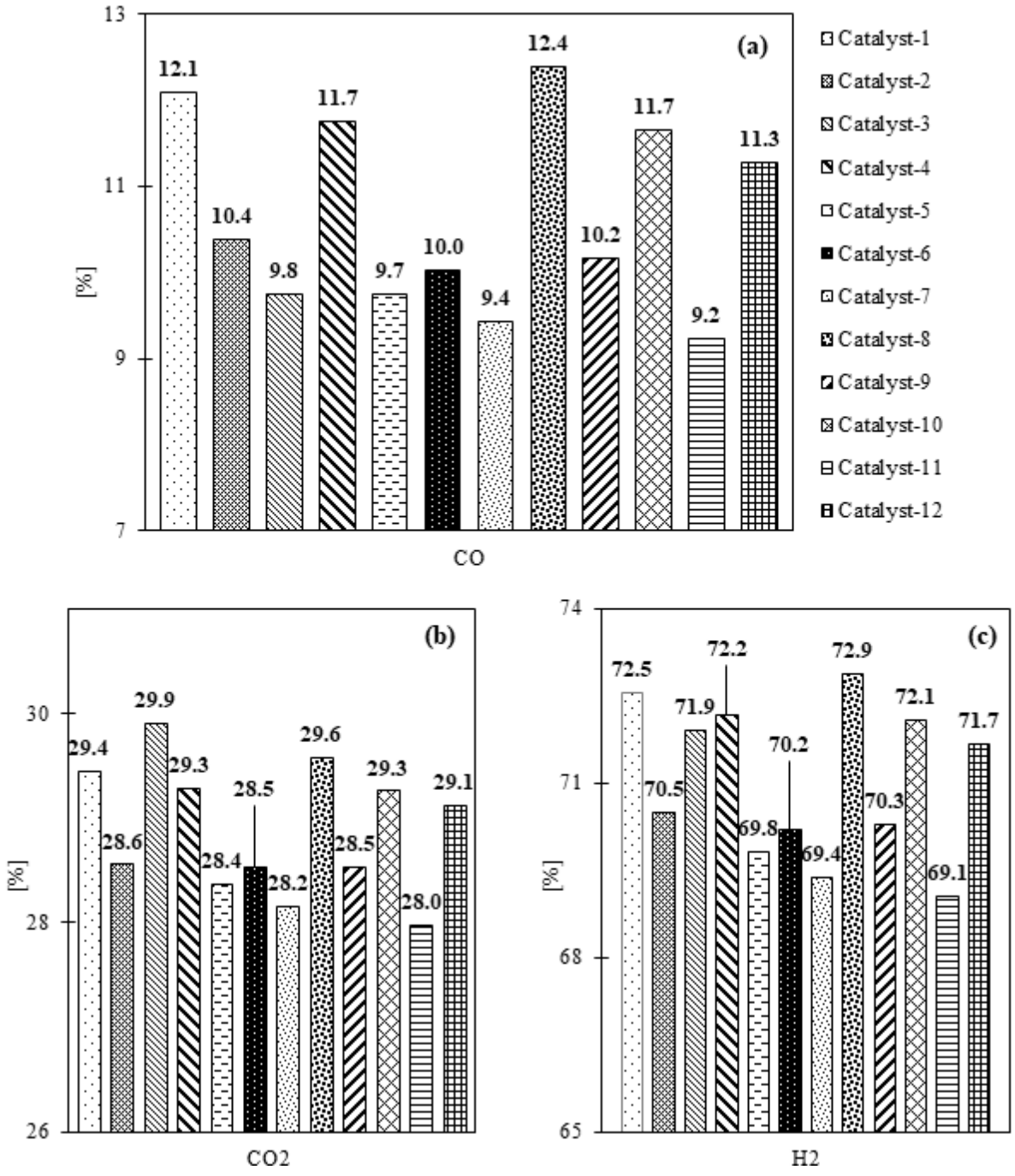

Fig. 9. Comparison of reforming catalysts in terms of a) CO selectivity; b) CO_2 selectivity; c) H_2 selectivity at 973 K, 30 bar, S/C of 3.0 and G_s of 3.5 kg $m^{-2}s^{-1}$. Equilibrium values were 13.7% for CO, 30.5% for CO_2 and 74.6% for H_2 selectivity respectively.

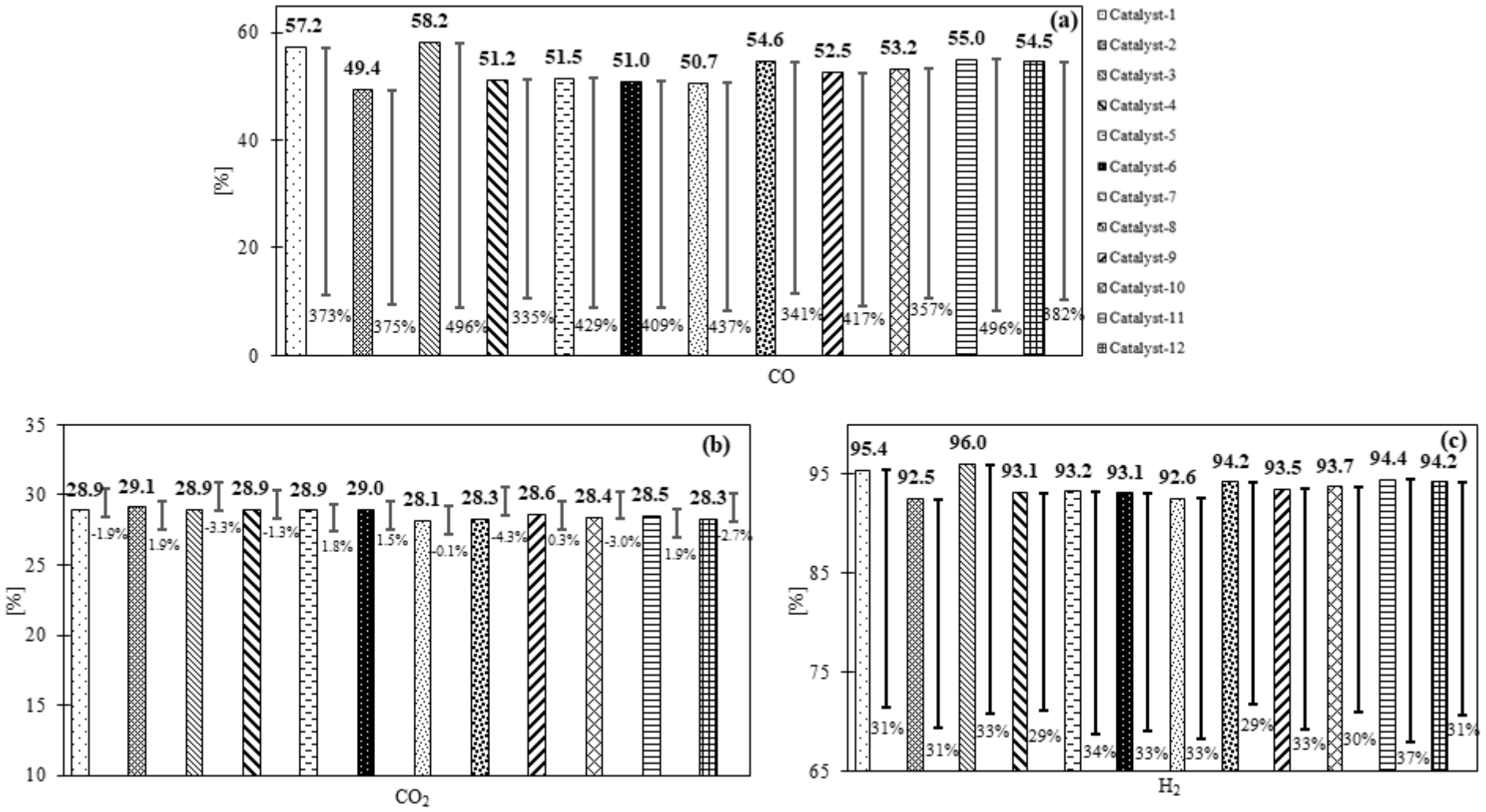

Fig. 10. Comparison of reforming catalysts in terms of a) CO selectivity; b) CO_2 selectivity; c) H_2 selectivity at 1173 K, 30 bar, S/C of 3.0 and G_s of 3.5 kg $m^{-2}s^{-1}$. Equilibrium values were 59.6% for CO, 29% for CO_2 and 96.3% for H_2 selectivity respectively. The % bars next to the pattern bars are in order from left to right (Catalyst-1 to Catalyst-12) and they represent the % increase or decrease when the temperature is increased from 973 K to 1173 K.

5.3 Thermal efficiency

A basic measure of the thermal efficiency of the primary reforming process based on lower heating value (LHV) as a function of the combined H_2 and CO yields is given by Eq. 15. The equation assumes complete subsequent conversion of the primary reformer's CO output into CO_2 via downstream WGS, with concurrent equimolar conversion of the H_2O co-feed to H_2 (see R2).

$$\text{Thermal efficiency (\%)} = \frac{\left(\text{LHV}_{\text{H}_2} \times \text{moles of H}_2\right) + \left(\text{LHV}_{\text{CO}} \times \text{moles of CO}\right)}{\text{LHV}_{\text{CH}_4} \times \text{moles of feed CH}_4} \times 100 \qquad (15)$$

Fig. 11 shows the thermal efficiency (%) of the reformer using various catalysts at 1173 K, 30 bar, S/C of 3.0 and with G_s of 3.5 kg $m^{-2}s^{-1}$. Under the same operating conditions, the equilibrium thermal efficiency is 109.4%. The higher the S/C and temperature, the higher the number of moles of H_2 produced as well as the higher the thermal efficiency.

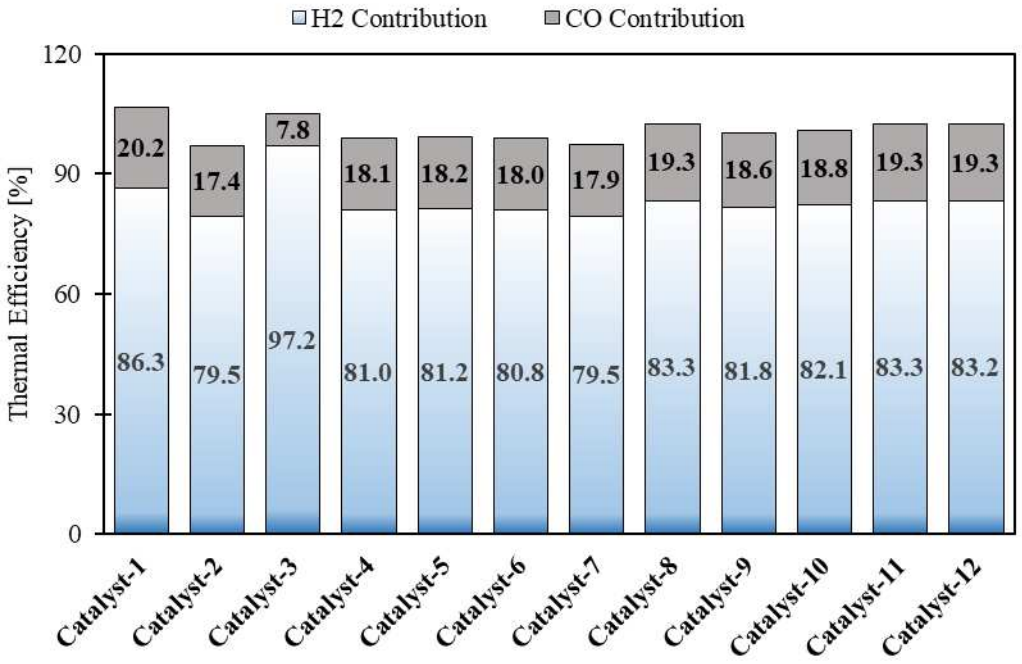

Fig. 11. Thermal efficiency of the reformer using various catalysts at 1173 K, 30 bar, S/C of 3.0 and G_s of 3.5 kg $m^{-2}s^{-1}$. Equilibrium yields a value of 109.4% for thermal efficiency under the same operating conditions.

The results presented in Fig. 11 reveal that catalyst-1 is the most thermally efficient catalyst with thermal efficiency value of 106.5%, closely followed by catalyst-3 with thermal efficiency of

105%. Both surpass all other catalysts in terms of efficiency because of their ability to give higher H_2 yield at the aforementioned operating conditions. Thermal efficiency greater than 100 can be justified by the endothermic nature of the process.

6. Conclusion

A 1-D dimensional heterogeneous mathematical model for an adiabatic fixed-bed reactor was used to compare the performance of eleven commercial catalysts used in the SMR process. The first order backward finite difference method was applied to solve the model system of PDAEs through gPROMS. The sensitivity analysis of the packed bed reactor model helped determine the best-operating conditions such as temperature, pressure, S/C, and G_s. The modelling results were found in good agreement with chemical equilibrium outputs based on the minimization of Gibbs free energy. Later, the modelling results were validated with results derived from industrial reforming conditions. At a fixed pressure, an increase in temperature produces an increase in CH_4 disappearance rate, H_2 yield (wt. % of CH_4), and H_2 purity, whilst at a fixed temperature, lowering the pressure results in the improvement of the CH_4 conversion. At 1 bar, when the temperature is increased above 973 K, there was no appreciable gain observed in the CH_4 conversion. It is concluded that at atmospheric pressure, 973 K is the optimum operating temperature for the SMR process although such low-pressure conditions are well known to be prohibitive for practical reasons (plant size and plant economics). According to the sensitivity of S/C values in the SMR process, which have an influence on coke deposition and operational cost, S/C of 3.0 was chosen as the optimum to get high values of CH_4 conversion and H_2 purity. The G_s of 3.5 kg $m^{-2}s^{-1}$ was selected as the optimal value for the SMR process. The sensitivity analysis reveals that the SMR process confirms the best performance at high temperature, low pressure and at larger values of S/C. The reactor model was then used for various catalysts to evaluate their performance under more realistic industrial operating conditions. A pressure of 30 bar, a S/C of 3 and G_s of 3.5 kg $m^{-2}s^{-1}$ was used to test the catalysts in two different scenarios of temperature, one in a mild temperatures of industrial conditions with a temperature of 973 K and the other in more severe industrial conditions with a temperature of 1173 K, with the anticipation that some catalysts may overtake others in activity. In regards to the catalysts performance, fast reaction kinetics gave better results under the set of operating conditions used. Catalyst-8, which is a Ni-based catalyst, showed superiority over all other catalysts in terms of CH_4 conversion, H_2 yield (wt. % of CH_4)

and H_2 purity with values of 42%, 19.7% and 60.9 % respectively at 973 K, 30 bar, S/C of 3 and G_s of 3.5 kg $m^{-2}s^{-1}$. Catalyst - 8 also provided the maximum H_2 and CO selectivity amongst all other catalysts due to its fast kinetics being active at 973 K and 30 bar. With the anticipation that some catalysts might show significant improvement in their performance at higher temperature, the reformer was simulated again with a different catalyst per run, but a fixed value of temperature (1173 K) and pressure (30 bar). Catalyst-3, which is also a Ni-based having NiO content of 15 – 17 wt. %, showed dominance over other catalysts by reaching 86.4% CH_4 conversion, 36.9% H_2 yield (wt. % of CH_4), and 74.4% H_2 purity at 1173 K, 30 bar, S/C of 3, and G_s of 3.5 kg $m^{-2}s^{-1}$. Owing to its slow kinetics at 973 K, Catalyst-11 was dominated by all other catalysts, but when the temperature was increased to 1173 K, it showed the maximum improvement in its performance (in terms of CH_4 conversion, H_2 yield, H_2 purity, and selectivity of C-based and H-based products) amongst all other catalysts. Hence, justifying that some catalysts might show different activity at different operating conditions. Catalyst-1, which is a commercial 15 wt. % Ni catalyst supported on magnesium spinel, exhibited a slightly better thermal efficiency in comparison to catalyst-3 but overall catalyst-3 dominated all other catalysts and showed better performance at 1173 K, 30 bar, and S/C of 3. In the present work, we have not considered the variation of operating variables into the network of pores of the catalyst. The scope of the proposed model confirms that is worthy of further development, and thus, it will be extended to simulate concentration and gas temperature changes intra-particle.

Moreover, plenty of literature exists on simulation studies of steam methane reforming using Xu and Froment [44] kinetic model; this model cannot be used as a generalized model, and plugging in that kinetic model to every catalyst might lead to false results and ambiguities. An approach to determine the kinetics with precision and in an efficient way is to equip a modeler with experimental tools and allow it to develop its own kinetics. This will automate the workflow of comparing the model against the experiment, which is currently being done manually, and thus it is time-consuming and prone to error. Recently, Gossler et al. [102] used the concept of an open software tool to analyze and derive the kinetics for the conversion of methane over rhodium catalysts. To understand the underlying reaction mechanism, the development of an adequate kinetic model is indispensable. Kinetic modelling remains a challenge because it demands expertise and the reliable thermodynamic and kinetic data from extensive costly experimentation.

A proper balance is inevitable between the level of details in the model and experimental information available. Devocht et al. [103] expanded the power-law model of Numaguchi and Kickuchi [43] over Langmuir–Hinshelwood–Hougen–Watson model to adjust the adsorption parameters and demonstrated the balance between the information available and the detail accounted for in the model. Catalysts manufactured for industrial use can strongly vary from laboratory-developed materials, thus the gap between the research and industrial catalysts must be exploited and one such effort was made by Mitchell et al [104], discussing the gap and the potential ways to bridge that gap between research and commercial catalysts.

Acknowledgments

Support from the University of Engineering and Technology, Lahore, Pakistan is gratefully acknowledged. We also thank the University of Leeds, UK for providing the license of gPROMS model builder 4.1.0® and making this research possible.

Nomenclature

$C_{p,bed}$	Heat capacity of the catalyst bed [J kg^{-1} K^{-1}]	G_s	Gas mass flow velocity [kg m^{-2} s^{-1}]
C_{pg}	Heat capacity of gases [J kg^{-1} K^{-1}]	ΔH_i	Heat of adsorption of i species [J mol^{-1}]
D_i	Effective diffusion coefficient [m^2 s^{-1}]	$H_{rxn,j}$	Heat of reaction of j reaction [J mol^{-1}]
D_m	Average molecular diffusivity [m^2 s^{-1}]	h_f	Gas to solid heat transfer coefficient [W m^{-2} s^{-1}]
P_i	Partial pressure of species i [bar]	j_D, j_H	Chilton-Colburn factor for mass and heat transfer
D_z	Axial dispersion coefficient [m^2 s^{-1}]	$k_{g,i}$	Gas to solid mass transfer coefficient of component i [m^3 m^{-2} s^{-1}]
d_p	Particle diameter [m]	k_j	Kinetic rate constant of reaction j
E_j	Activation energy of reaction j [J mol^{-1}]	k_{oj}	Reference temperature dependent kinetic rate constant of reaction j
G	Gibbs free energy [J]	K_j	Thermodynamic equilibrium constant
LHV_{H_2}	Lower heating value of H_2 [J mol^{-1}]	K_i	Adsorption constant of species i
LHV_{CH_4}	Lower heating value of CH_4 [J mol^{-1}]	K_{oi}	Reference adsorption constant of species i
P	Total gas pressure [bar]	T	Gas temperature [K]
Pr	Prandtl number	u	Superficial velocity of the gases [m s^{-1}]
Ri	Rate of formation or consumption of species i [mol kg_{cat}^{-1} s^{-1}]	Sc_i	Schmidt number
R_j	Rate of reaction j [mol kg_{cat}^{-1} s^{-1}]	z	Axial dimension [m]
R_g	Ideal gas constant [J mol^{-1} K^{-1}]	Re	Reynolds number

Greek letters

Ω	Unit less dominator term in the reaction kinetics	λ_z^f	Effective thermal conductivity [W m^{-1} K^{-1}]

ε_b	Packing bed porosity	μ_g	Average gas viscosity [kg m^{-1} s^{-1}]
η_j	Effectiveness factor of reaction j	ρ_{bed}	density of the catalyst bed [kg m^{-3}]
λ_g	Average gas thermal conductivity [W m^{-1} K^{-1}]	ρ_{cat}	density of the catalyst pellet [kg m^{-3}]
λ_s	Solid thermal conductivity [W m^{-1} K^{-1}]	ρ_f	Fluid density [kg m^{-3}]

Appendix A

The kinetic rate equations and kinetic parameters used in the reactor model:

$$R_1 = \frac{k_1}{p_{H_2}^{2.5}}\left(p_{CH_4}p_{H_2O} - \frac{p_{H_2}^3 p_{CO}}{K_I}\right)\left(\frac{1}{\Omega^2}\right) \quad (A.1)$$

$$R_2 = \frac{k_3}{p_{H_2}}\left(p_{co}p_{H_2O} - \frac{p_{H_2}p_{CO}}{K_{II}}\right)\left(\frac{1}{\Omega^2}\right) \quad (A.2)$$

$$R_3 = \frac{k_2}{p_{H_2}^{3.5}}\left(p_{CH_4}p_{H_2O}^2 - \frac{p_{H_2}^4 p_{CO_2}}{K_{III}}\right)\left(\frac{1}{\Omega^2}\right) \quad (A.3)$$

$$\Omega = 1 + K_{CO}p_{CO} + K_{H_2}p_{H_2} + K_{CH_4}p_{HCH_4} + K_{H_2O}\frac{p_{H_2O}}{p_{H_2}} \quad (A.4)$$

$$R_1 = \frac{k_1}{p_{H_2}^{1.25}}\left(p_{CH_4}\, p_{H_2O}^{0.5} - \frac{p_{H_2}^3 p_{CO}}{K_I\, p_{H_2O}^{0.5}}\right)\left(\frac{1}{\Omega^2}\right) \quad (A.5)$$

$$R_2 = \frac{k_2}{p_{H_2}^{0.5}}\left(p_{CO}\, p_{H_2O}^{0.5} - \frac{p_{H_2}p_{CO_2}}{K_{II}\, p_{H_2O}^{0.5}}\right)\left(\frac{1}{\Omega^2}\right) \quad (A.6)$$

$$R_3 = \frac{k_3}{p_{H_2}^{1.75}}\left(p_{CH_4}\, p_{H_2O} - \frac{p_{H_2}^4 p_{CO_2}}{K_{III}\, p_{H_2O}}\right)\left(\frac{1}{\Omega^2}\right) \quad (A.7)$$

$$\Omega = 1 + K_{CO}\, p_{CO} + K_{H_2}\, p_{H_2}^{0.5} + K_{H_2O}\frac{p_{H_2O}}{p_{H_2}} \quad (A.8)$$

$$R_1 = \frac{k_1}{p_{H_2}^{2.5}}\left(p_{CH_4}p_{H_2O} - \frac{p_{H_2}^3 p_{CO}}{K_I}\right) \times \Omega_1\Omega_S \quad (A.9)$$

$$R_2 = \frac{k_2}{p_{H_2}}\left(p_{CO}p_{H_2O} - \frac{p_{H_2}p_{CO_2}}{K_{II}}\right) \times \Omega_1\Omega_S \quad (A.10)$$

$$R_3 = \frac{k_3}{p_{H_2}^{3.5}}\left(p_{CH_4}p_{H_2O}^2 - \frac{p_{H_2}^4 p_{CO_2}}{K_{III}}\right) \times \Omega_1\Omega_S \quad (A.11)$$

$$\Omega_1 = \frac{1}{1 + K_{CH_4}p_{CH_4}/{p_{H_2}}^{0.5} + K_{CO}p_{CO} + K_{CO_2}p_{CO_2} + K_{H_2}p_{H_2}} \quad (A.12)$$

$$\Omega_S = \frac{1}{1 + K_{H_2O}p_{H_2O}/p_{H_2} + K_{H_2}p_{H_2}} \quad (A.13)$$

$$K_I = \exp\left(\frac{-26830}{T_s} + 30.114\right) \quad (A.14)$$

$$K_{II} = \exp\left(\frac{4400}{T_s} - 4.036\right) \quad (A.15)$$

$$K_{III} = K_I K_{II} \quad (A.16)$$

$$k_j = k_{oj}\exp\left(\frac{-E_j}{R_g T}\right) \quad (A.17)$$

$$K_i = K_{oi}\exp\left(\frac{-\Delta H_i}{R_g T}\right) \quad (A.18)$$

$$R_1 = \frac{k_1}{p_{H_2O}^{0.596}}\left(p_{CH_4}p_{H_2O} - \frac{p_{H_2}^3 p_{CO}}{K_I}\right) \quad (A.19)$$

$$R_2 = k_2\left(p_{co}p_{H_2O} - \frac{p_{H_2}p_{CO_2}}{K_{II}}\right) \quad (A.20)$$

Appendix B

Physical properties are estimated by using the following empirical correlations:

Effective thermal conductivity is given as [105];

$$\frac{\lambda_z^f}{\lambda_g} = \frac{\lambda_z^o}{\lambda_g} + 0.75 \mathrm{Pr} \mathrm{Re}_p \tag{B.1}$$

$$\frac{\lambda_z^o}{\lambda_g} = \varepsilon_b + \frac{1-\varepsilon_b}{0.139\varepsilon_b - 0.0339 + \left(\frac{2}{3}\right)\lambda_g/\lambda_s} \tag{B.2}$$

Axial mass dispersion coefficient is defined is expressed as [106];

$$D_z = 0.73 D_m + \frac{0.5 u d_p}{1 + 9.49\, D_m/u d_p} \tag{B.3}$$

The mass transfer coefficient is given by the following relation [107];

$$k_{g,i} = j_{D,i} \mathrm{Re}_p \mathrm{Sc}_i^{1/3} \frac{D_i}{d_p} \tag{B.4}$$

$$k_{g,i} = j_{D,i} {\mathrm{Re}_p}^{-0.82} + 0.365 \mathrm{Sc}_i^{-0.398} \tag{B.5}$$

The dimensionless numbers are given as;

$$\mathrm{Re}_p = \frac{\rho_g u d_p}{\mu} \; ; \; 0.01 < \mathrm{Re}_p < 1500 \tag{B.6}$$

$$\mathrm{Sc}_i = \frac{\mu}{\rho_g D_i} \; ; \; 0.6 < \mathrm{Sc} < 7000 \, , 0.25 < \varepsilon_b < 0.96 \tag{B.7}$$

Heat transfer coefficient and its dimensionless numbers are given by the following expressions [107, 108];

$$h_f = j_H \frac{C_{pg} G_s}{\mathrm{Pr}^{2/3}} \tag{B.8}$$

$$j_H = 0.91 {\mathrm{Re}_p}^{-0.51} \psi \; ; \; 0.01 < \mathrm{Re}_p < 50 \tag{B.9}$$

$$j_H = 0.61 {\mathrm{Re}_p}^{-0.41} \psi \; ; \; 50 < \mathrm{Re}_p < 1000 \tag{B.10}$$

$$\mathrm{Pr} = \frac{C_{pg}\mu_g}{\lambda_g} \quad \text{(B.11)}$$

References

1. M.C. Sánchez-Sánchez, R.M. Navarro and J.L.G. Fierro, Ethanol steam reforming over Ni/La–Al2O3 catalysts: Influence of lanthanum loading. Catalysis Today, 2007. **129**(3): p. 336-345.
2. I. Dincer and C. Acar, Review and evaluation of hydrogen production methods for better sustainability. International Journal of Hydrogen Energy, 2015. **40**(34): p. 11094-11111.
3. B. Parkinson, et al., Hydrogen production using methane: Techno-economics of decarbonizing fuels and chemicals. International Journal of Hydrogen Energy, 2018. **43**(5): p. 2540-2555.
4. W. McDowall and M. Eames, Forecasts, scenarios, visions, backcasts and roadmaps to the hydrogen economy: A review of the hydrogen futures literature. Energy Policy, 2006. **34**(11): p. 1236-1250.
5. S. Sharma and S.K. Ghoshal, Hydrogen the future transportation fuel: From production to applications. Renewable and Sustainable Energy Reviews, 2015. **43**: p. 1151-1158.
6. D. Eliezer, N. Eliaz, O.N. Senkov and F.H. Froes, Positive effects of hydrogen in metals. Materials Science and Engineering: A, 2000. **280**(1): p. 220-224.
7. V. Dupont, Steam reforming of sunflower oil for hydrogen gas production. Vol. 30. 2007. 103-132.
8. M. Momirlan and T.N. Veziroglu, The properties of hydrogen as fuel tomorrow in sustainable energy system for a cleaner planet. International journal of hydrogen energy, 2005. **30**(7): p. 795-802.
9. M.K. Nikoo, S. Saeidi, A.J.C.T. Lohi and E. Policy, A comparative thermodynamic analysis and experimental studies on hydrogen synthesis by supercritical water gasification of glucose. 2015. **17**(8): p. 2267-2288.
10. H. Balat and E. Kırtay, Hydrogen from biomass–present scenario and future prospects. International Journal of Hydrogen Energy, 2010. **35**(14): p. 7416-7426.
11. A. Zamaniyan, A. Behroozsarand and H. Ebrahimi, Modeling and simulation of large scale hydrogen production. Journal of Natural Gas Science and Engineering, 2010. **2**(6): p. 293-301.
12. A. Iulianelli, S. Liguori, J. Wilcox and A. Basile, Advances on methane steam reforming to produce hydrogen through membrane reactors technology: A review. Catalysis Reviews, 2016. **58**(1): p. 1-35.
13. M. Balat and M. Balat, Political, economic and environmental impacts of biomass-based hydrogen. International Journal of Hydrogen Energy, 2009. **34**(9): p. 3589-3603.

14. N.Z. Muradov and T.N. Veziroğlu, From hydrocarbon to hydrogen–carbon to hydrogen economy. International Journal of Hydrogen Energy, 2005. **30**(3): p. 225-237.
15. M.A. Rosen, Thermodynamic investigation of hydrogen production by steam-methane reforming. International Journal of Hydrogen Energy, 1991. **16**(3): p. 207-217.
16. A.M. Adris, B.B. Pruden, C.J. Lim and J.R. Grace, On the reported attempts to radically improve the performance of the steam methane reforming reactor. The Canadian Journal of Chemical Engineering, 1996. **74**(2): p. 177-186.
17. J. Pasel, R.C. Samsun, A. Tschauder, R. Peters and D. Stolten, A novel reactor type for autothermal reforming of diesel fuel and kerosene. Applied energy, 2015. **150**: p. 176-184.
18. M. Farsi and H. Shahhosseini, A modified membrane SMR reactor to produce large-scale syngas: modeling and multi objective optimization. Chemical Engineering and Processing: Process Intensification, 2015. **97**: p. 169-179.
19. B. Metz, O. Davidson, H.d. Coninck, M. Loos and L. Meyer, IPPC Special Report on Carbon Dioxide Capture and Storage, Intergovernmental Panel on Climate Change. Cambridge University Press, 2005.
20. M. Boaro, S. Colussi and A. Trovarelli, Ceria-based materials in hydrogenation and reforming reactions for CO2 valorization. Frontiers in chemistry, 2019. **7**: p. 28.
21. D.P. Harrison, Sorption-enhanced hydrogen production: a review. Industrial & engineering chemistry research, 2008. **47**(17): p. 6486-6501.
22. W. Roger, Hydrogen production. 1933, Google Patents.
23. B. Balasubramanian, A.L. Ortiz, S. Kaytakoglu and D.P. Harrison, Hydrogen from methane in a single-step process. Chemical Engineering Science, 1999. **54**(15-16): p. 3543-3552.
24. A. Lopez Ortiz and D.P. Harrison, Hydrogen production using sorption-enhanced reaction. Industrial & engineering chemistry research, 2001. **40**(23): p. 5102-5109.
25. D.K. Lee, I.H. Baek and W.L. Yoon, Modeling and simulation for the methane steam reforming enhanced by in situ CO2 removal utilizing the CaO carbonation for H2 production. Chemical Engineering Science, 2004. **59**(4): p. 931-942.
26. K.B. Yi and D.P. Harrison, Low-pressure sorption-enhanced hydrogen production. Industrial & engineering chemistry research, 2005. **44**(6): p. 1665-1669.
27. Y.I. Yoon, I.H. Baek and S. Do Park, Enhancement of H2 production by combination with CO2 absorption in steam methane reforming in bench scale. Journal of Industrial and Engineering Chemistry, 2007. **13**(5): p. 842-849.
28. Z.-s. Li and N.-s. Cai, Modeling of multiple cycles for sorption-enhanced steam methane reforming and sorbent regeneration in fixed bed reactor. Energy & Fuels, 2007. **21**(5): p. 2909-2918.

29. A.I. Lysikov, S.N. Trukhan and A.G. Okunev, Sorption enhanced hydrocarbons reforming for fuel cell powered generators. International journal of hydrogen energy, 2008. **33**(12): p. 3061-3066.
30. C.S. Martavaltzi and A.A. Lemonidou, Hydrogen production via sorption enhanced reforming of methane: Development of a novel hybrid material—reforming catalyst and CO2 sorbent. Chemical Engineering Science, 2010. **65**(14): p. 4134-4140.
31. A. Di Giuliano, et al., Sorption enhanced steam methane reforming by Ni/CaO/mayenite combined systems: Overview of experimental results from E uropean research project ASCENT. The Canadian Journal of Chemical Engineering, 2020. **98**(9): p. 1907-1923.
32. T. Mattisson, A. Järdnäs and A. Lyngfelt, Reactivity of some metal oxides supported on alumina with alternating methane and oxygen application for chemical-looping combustion. Energy & Fuels, 2003. **17**(3): p. 643-651.
33. S. Noorman, M. van Sint Annaland and H. Kuipers, Packed bed reactor technology for chemical-looping combustion. Industrial & Engineering Chemistry Research, 2007. **46**(12): p. 4212-4220.
34. A. Abad, J. Adánez, F. García-Labiano, F. Luis and P. Gayán, Modeling of the chemical-looping combustion of methane using a Cu-based oxygen-carrier. Combustion and flame, 2010. **157**(3): p. 602-615.
35. J.C. Abanades, R. Murillo, J.R. Fernandez, G. Grasa and I. Martínez, New CO2 capture process for hydrogen production combining Ca and Cu chemical loops. Environmental science & technology, 2010. **44**(17): p. 6901-6904.
36. J.R. Fernández, J.C. Abanades, R. Murillo and G. Grasa, Conceptual design of a hydrogen production process from natural gas with CO2 capture using a Ca–Cu chemical loop. International Journal of Greenhouse Gas Control, 2012. **6**: p. 126-141.
37. T.L. LeValley, A.R. Richard and M. Fan, The progress in water gas shift and steam reforming hydrogen production technologies – A review. International Journal of Hydrogen Energy, 2014. **39**(30): p. 16983-17000.
38. G. Jones, et al., First principles calculations and experimental insight into methane steam reforming over transition metal catalysts. Journal of Catalysis, 2008. **259**(1): p. 147-160.
39. X. Guo, Y. Sun, Y. Yu, X. Zhu and C.-j. Liu, Carbon formation and steam reforming of methane on silica supported nickel catalysts. Catalysis Communications, 2012. **19**: p. 61-65.
40. J.R. Rostrup-Nielsen, Catalytic steam reforming, in Catalysis. 1984, Springer. p. 1-117.
41. M.V. Twigg, Catalyst handbook. 2018: Routledge.
42. W.W. Akers and D.P. Camp, Kinetics of the methane-steam reaction. AIChE Journal, 1955. **1**(4): p. 471-475.
43. T. Numaguchi and K. Kikuchi, Intrinsic kinetics and design simulation in a complex reaction

network; steam-methane reforming. Chemical Engineering Science, 1988. **43**(8): p. 2295-2301.

44. J. Xu and G.F. Froment, Methane steam reforming, methanation and water-gas shift: I. Intrinsic kinetics. AIChE Journal, 1989. **35**(1): p. 88-96.
45. M.A. Soliman, A.M. Adris, A.S. Al-Ubaid and S.S.E.H. El-Nashaie, Intrinsic kinetics of nickel/calcium aluminate catalyst for methane steam reforming. Journal of Chemical Technology & Biotechnology, 1992. **55**(2): p. 131-138.
46. A.C. Luna, A.J.R.K. Becerra and C. Letters, Kinetics of methane steam reforming on a Ni on alumina-titania catalyst. 1997. **61**(2): p. 369-374.
47. K. Hou and R. Hughes, The kinetics of methane steam reforming over a Ni/α-Al2O catalyst. Chemical Engineering Journal, 2001. **82**(1): p. 311-328.
48. C. McGreavy and M. Newmann. Development of a mathematical model of a steam methane reformer. in Institution of Electrical Engineering, Conference on the Industrial Applications of Dynamic Modelling. 1969.
49. C.P.P. Singh and D.N. Saraf, Simulation of Low-Temperature Water-Gas Shift Reactor. Industrial & Engineering Chemistry Process Design and Development, 1980. **19**(3): p. 393-396.
50. J. Xu and G.F. Froment, Methane steam reforming: II. Diffusional limitations and reactor simulation. AIChE Journal, 1989. **35**(1): p. 97-103.
51. M.A. Soliman, S.S.E.H. El-Nashaie, A.S. Al-Ubaid and A. Adris, Simulation of steam reformers for methane. Chemical Engineering Science, 1988. **43**(8): p. 1801-1806.
52. C.V.S. Murty and M.V.K. Murthy, Modeling and simulation of a top-fired reformer. Industrial & Engineering Chemistry Research, 1988. **27**(10): p. 1832-1840.
53. P.M. Plehiers and G.F. Froment, Coupled simulation of heat transfer and reaction in a steam reforming furnace. Chemical Engineering & Technology, 1989. **12**(1): p. 20-26.
54. Z. Yu, E. Cao, Y. Wang, Z. Zhou and Z. Dai, Simulation of natural gas steam reforming furnace. Fuel Processing Technology, 2006. **87**(8): p. 695-704.
55. J. Shayegan, M.M.Y.M. Hashemi and K. Vakhshouri, Operation of an industrial steam reformer under severe condition: A simulation study. The Canadian Journal of Chemical Engineering, 2008. **86**(4): p. 747-755.
56. H. Ebrahimi, J.S.S. Mohammadzadeh, A. Zamaniyan and F. Shayegh, Effect of design parameters on performance of a top fired natural gas reformer. Applied Thermal Engineering, 2008. **28**(17): p. 2203-2211.
57. A. Olivieri and F. Vegliò, Process simulation of natural gas steam reforming: Fuel distribution optimisation in the furnace. Fuel Processing Technology, 2008. **89**(6): p. 622-632.
58. S.Z. Abbas, V. Dupont and T. Mahmud, Kinetics study and modelling of steam methane reforming

process over a NiO/Al2O3 catalyst in an adiabatic packed bed reactor. International Journal of Hydrogen Energy, 2017. **42**(5): p. 2889-2903.

59. P.B. Weisz and C.D. Prater, Interpretation of measurements in experimental catalysis. Adv. Catal, 1954. **6**(143): p. 60390-9.
60. H.S. Fogler, Essentials of Chemical Reaction Engineering. 2010: Pearson Education.
61. G.F. Froment, K.B. Bischoff and J. De Wilde, Chemical reactor analysis and design. Vol. 2. 1990: Wiley New York.
62. B.T. Schädel, M. Duisberg and O. Deutschmann, Steam reforming of methane, ethane, propane, butane, and natural gas over a rhodium-based catalyst. Catalysis today, 2009. **142**(1-2): p. 42-51.
63. I. Champon, A. Bengaouer, A. Chaise, S. Thomas and A.-C. Roger, Carbon dioxide methanation kinetic model on a commercial Ni/Al2O3 catalyst. Journal of CO2 Utilization, 2019. **34**: p. 256-265.
64. M.M. Hossain and H.I. de Lasa, Reactivity and stability of Co-Ni/Al2O3 oxygen carrier in multicycle CLC. AIChE Journal, 2007. **53**(7): p. 1817-1829.
65. H. Jin and M. Ishida, Reactivity Study on Natural-Gas-Fueled Chemical-Looping Combustion by a Fixed-Bed Reactor. Industrial & Engineering Chemistry Research, 2002. **41**(16): p. 4004-4007.
66. M. Rydén, A. Lyngfelt and T. Mattisson, Synthesis gas generation by chemical-looping reforming in a continuously operating laboratory reactor. Fuel, 2006. **85**(12): p. 1631-1641.
67. D.L. Hoang, S.H. Chan and O.L. Ding, Kinetic and modelling study of methane steam reforming over sulfide nickel catalyst on a gamma alumina support. Chemical Engineering Journal, 2005. **112**(1): p. 1-11.
68. E.L.G. Oliveira, C.A. Grande and A.E. Rodrigues, Methane steam reforming in large pore catalyst. Chemical Engineering Science, 2010. **65**(5): p. 1539-1550.
69. E.L.G. Oliveira, C.A. Grande and A.E. Rodrigues, Steam methane reforming in a Ni/Al2O3 catalyst: Kinetics and diffusional limitations in extrudates. The Canadian Journal of Chemical Engineering, 2009. **87**(6): p. 945-956.
70. M.H. Halabi, M.H.J.M. de Croon, J. van der Schaaf, P.D. Cobden and J.C. Schouten, Intrinsic kinetics of low temperature catalytic methane–steam reforming and water–gas shift over Rh/CeαZr1−αO2 catalyst. Applied Catalysis A: General, 2010. **389**(1): p. 80-91.
71. C. Kanhari, T. Vatanatham and S. Limtrakul, Kinetic Rates of Steam-Methane Reforming over Ni / Al_2O_3 catalyst. Kasetsart Engineering Journal, 2013. **85**(1): p. 53-62.
72. A. Obradović, B. Likozar and J. Levec, Steam Methane Reforming over Ni-based Pellet-type and Pt/Ni/Al2O3 Structured Plate-type Catalyst: Intrinsic Kinetics Study. Industrial & Engineering Chemistry Research, 2013. **52**(38): p. 13597-13606.

73. C.N. Ávila-Neto, et al., Hydrogen production from methane reforming: Thermodynamic assessment and autothermal reactor design. Journal of Natural Gas Science and Engineering, 2009. **1**(6): p. 205-215.
74. A.C.D. Freitas and R. Guirardello, Thermodynamic analysis of methane reforming with CO2, CO2+H2O, CO2+O2 and CO2+air for hydrogen and synthesis gas production. Journal of CO2 Utilization, 2014. **7**: p. 30-38.
75. Ş. Özkara-Aydınoğlu, Thermodynamic equilibrium analysis of combined carbon dioxide reforming with steam reforming of methane to synthesis gas. International Journal of Hydrogen Energy, 2010. **35**(23): p. 12821-12828.
76. Y. Li, Y. Wang, X. Zhang and Z. Mi, Thermodynamic analysis of autothermal steam and CO2 reforming of methane. International Journal of Hydrogen Energy, 2008. **33**(10): p. 2507-2514.
77. J.R. Rostrup-Nielsen, Industrial relevance of coking. Catalysis Today, 1997. **37**(3): p. 225-232.
78. D.L. Trimm, Coke formation and minimisation during steam reforming reactions. Catalysis Today, 1997. **37**(3): p. 233-238.
79. J.R. Rostrup-Nielsen, New aspects of syngas production and use. Catalysis today, 2000. **63**(2-4): p. 159-164.
80. H. Uchida and M.R. Harada, Hydrogen Energy Engineering Applications and Products, in Science and Engineering of Hydrogen-Based Energy Technologies. 2019, Elsevier. p. 201-220.
81. C.H. Bartholomew, Carbon deposition in steam reforming and methanation. Catalysis Reviews Science and Engineering, 1982. **24**(1): p. 67-112.
82. G.C. Bond, The role of carbon deposits in metal-catalysed reactions of hydrocarbons. Applied Catalysis A: General, 1997. **149**(1): p. 3-25.
83. J.R. Rostrup-Nielsen and J. Sehested, Whisker carbon revisited, in Studies in Surface Science and Catalysis. 2001, Elsevier. p. 1-12.
84. D.L. Trimm, The formation and removal of coke from nickel catalyst. Catalysis Reviews Science and Engineering, 1977. **16**(1): p. 155-189.
85. Y.H. Hu and E. Ruckenstein, Catalytic conversion of methane to synthesis gas by partial oxidation and CO2 reforming. ChemInform, 2004. **35**(49): p. no-no.
86. H.-S. Roh and K.-W. Jun, Carbon dioxide reforming of methane over Ni catalysts supported on Al 2 O 3 modified with La 2 O 3, MgO, and CaO. Catalysis surveys from Asia, 2008. **12**(4): p. 239-252.
87. B. Huang, et al., Effect of MgO promoter on Ni-based SBA-15 catalysts for combined steam and carbon dioxide reforming of methane. Journal of natural gas chemistry, 2008. **17**(3): p. 225-231.
88. S.O. Choi and S.H. Moon, Performance of La1− xCexFe0. 7Ni0. 3O3 perovskite catalysts for

methane steam reforming. Catalysis Today, 2009. **146**(1-2): p. 148-153.

89. G.S. Gallego, C. Batiot-Dupeyrat, J. Barrault, E. Florez and F. Mondragon, Dry reforming of methane over LaNi1− yByO3±δ (B= Mg, Co) perovskites used as catalyst precursor. Applied Catalysis A: General, 2008. **334**(1-2): p. 251-258.
90. R. Pereñíguez, V.M. González-DelaCruz, J.P. Holgado and A. Caballero, Synthesis and characterization of a LaNiO3 perovskite as precursor for methane reforming reactions catalysts. Applied Catalysis B: Environmental, 2010. **93**(3-4): p. 346-353.
91. I. Rivas, J. Alvarez, E. Pietri, M.J. Pérez-Zurita and M.R. Goldwasser, Perovskite-type oxides in methane dry reforming: Effect of their incorporation into a mesoporous SBA-15 silica-host. Catalysis Today, 2010. **149**(3-4): p. 388-393.
92. V.M. Gonzalez-DelaCruz, J.P. Holgado, R. Pereñíguez and A. Caballero, Morphology changes induced by strong metal–support interaction on a Ni–ceria catalytic system. Journal of Catalysis, 2008. **257**(2): p. 307-314.
93. V.M. Gonzalez-Delacruz, F. Ternero, R. Pereñíguez, A. Caballero and J.P. Holgado, Study of nanostructured Ni/CeO2 catalysts prepared by combustion synthesis in dry reforming of methane. Applied Catalysis A: General, 2010. **384**(1-2): p. 1-9.
94. B. Fidalgo, L. Zubizarreta, J.M. Bermúdez, A. Arenillas and J.A. Menéndez, Synthesis of carbon-supported nickel catalysts for the dry reforming of CH4. Fuel Processing Technology, 2010. **91**(7): p. 765-769.
95. L. Chen, Q. Zhu, Z. Hao, T. Zhang and Z. Xie, Development of a Co–Ni bimetallic aerogel catalyst for hydrogen production via methane oxidative CO2 reforming in a magnetic assisted fluidized bed. international journal of hydrogen energy, 2010. **35**(16): p. 8494-8502.
96. L. Oukacine, F. Gitzhofer, N. Abatzoglou and D. Gravelle, Application of the induction plasma to the synthesis of two dimensional steam methane reforming Ni/Al2O3 catalyst. Surface and Coatings Technology, 2006. **201**(5): p. 2046-2053.
97. L. Wang, X. Ao and S. Wang, Catalysts for carbon dioxide catalytic reforming of methane to synthesis gas. Progress in Chemistry, 2012(9): p. 1696.
98. C.A. Bernardo and D.L. Trimm, The kinetics of gasification of carbon deposited on nickel catalysts. Carbon, 1979. **17**(2): p. 115-120.
99. M. Seemann and H. Thunman, Methane synthesis, in Substitute Natural Gas from Waste. 2019, Elsevier. p. 221-243.
100. A.E. Lutz, R.W. Bradshaw, J.O. Keller and D.E. Witmer, Thermodynamic analysis of hydrogen production by steam reforming. International Journal of Hydrogen Energy, 2003. **28**(2): p. 159-167.

101. J.R. Rostrup-Nielsen, J. Sehested and J.K. Nørskov, Hydrogen and synthesis gas by steam- and C02 reforming, in Advances in Catalysis. 2002, Academic Press. p. 65-139.
102. H. Gossler, L. Maier, S. Angeli, S. Tischer and O. Deutschmann, CaRMeN: a tool for analysing and deriving kinetics in the real world. Physical Chemistry Chemical Physics, 2018. **20**(16): p. 10857-10876.
103. B.R. Devocht, et al., Balance between model detail and experimental information in steam methane reforming o ver a Ni/MgO-SiO2 catalyst. AIChE Journal, 2019. **65**(4): p. 1222-1233.
104. S. Mitchell, N.-L. Michels and J. Pérez-Ramírez, From powder to technical body: the undervalued science of catalyst scale up. Chemical Society Reviews, 2013. **42**(14): p. 6094-6112.
105. S. Yagi, D. Kunii and N. Wakao, Studies on axial effective thermal conductivities in packed beds. AIChE Journal, 1960. **6**(4): p. 543-546.
106. M.F. Edwards and J.F. Richardson, Gas dispersion in packed beds. Chemical Engineering Science, 1968. **23**(2): p. 109-123.
107. C.J.N. Geankoplis, MA, Transport Processes and Unit Operations. Allyn and Bacon. 1995.
108. D. Handley and P.J. Heggs, The effect of thermal conductivity of the packing material on transient heat transfer in a fixed bed. International Journal of Heat and Mass Transfer, 1969. **12**(5): p. 549-570.